



**HAL**  
open science

# On the structural stiffness maximisation of anisotropic continua under inhomogeneous Neumann-Dirichlet boundary conditions

Marco Montemurro

► **To cite this version:**

Marco Montemurro. On the structural stiffness maximisation of anisotropic continua under inhomogeneous Neumann-Dirichlet boundary conditions. *Composite Structures*, 2022, 287, pp.115289. 10.1016/j.compstruct.2022.115289 . hal-03602403

**HAL Id: hal-03602403**

**<https://hal.science/hal-03602403v1>**

Submitted on 22 Jul 2024

**HAL** is a multi-disciplinary open access archive for the deposit and dissemination of scientific research documents, whether they are published or not. The documents may come from teaching and research institutions in France or abroad, or from public or private research centers.

L'archive ouverte pluridisciplinaire **HAL**, est destinée au dépôt et à la diffusion de documents scientifiques de niveau recherche, publiés ou non, émanant des établissements d'enseignement et de recherche français ou étrangers, des laboratoires publics ou privés.



Distributed under a Creative Commons Attribution - NonCommercial 4.0 International License

# On the structural stiffness maximisation of anisotropic continua under inhomogeneous Neumann-Dirichlet boundary conditions

M. Montemurro<sup>a,\*</sup>

<sup>a</sup>Arts et Métiers Institute of Technology, Université de Bordeaux, CNRS, INRA, Bordeaux INP, HESAM Université, I2M UMR 5295, F-33405 Talence, France

---

## Abstract

This work discusses three aspects of topology optimisation (TO) problems dealing with structural stiffness maximisation of anisotropic continua under mixed inhomogeneous Neumann-Dirichlet boundary conditions (BCs). Firstly, the total potential energy (TPE) is introduced as intuitive measure of the structural stiffness instead of the work of applied forces and displacements (WAFD). Secondly, it is proven that the WAFD under mixed BCs is not a self-adjoint functional, while the one related to the TPE is always a self-adjoint functional, regardless of the BCs nature. Thirdly, the influence of the anisotropy, of the applied BCs and of the design requirement on the volume fraction on the optimised topology is investigated: depending on these features, the optimal solutions of the two problem formulations, i.e., minimisation of the TPE or minimisation of the WAFD subject to a constraint on the volume fraction, can coincide. The problem is formulated in the context of a special density-based TO approach wherein a Non-Uniform Rational Basis Spline (NURBS) hyper-surface is used to represent the topological descriptor, i.e., the pseudo-density field. The properties of NURBS entities are efficiently exploited to derive the gradient of the physical responses involved in the problem formulation and to easily satisfy the minimum length scale requirement (related to manufacturing needs). The differences between TPE-based and WAFD-based formulations and the effectiveness of the proposed method are shown on 2D and 3D problems.

*Keywords:* Topology optimisation, Mixed boundary conditions, Anisotropy, NURBS hyper-surfaces, Finite element method, Density-based method.

---

\*Corresponding author. Tel.: +33 55 68 45 422, Fax.: +33 54 00 06 964.

Email address: [marco.montemurro@ensam.eu](mailto:marco.montemurro@ensam.eu), [marco.montemurro@u-bordeaux.fr](mailto:marco.montemurro@u-bordeaux.fr) (M. Montemurro)

## Acronyms

<b>AM</b> additive manufacturing	<b>LSM</b> level set method
<b>BK1-2D</b> first 2D benchmark problem	<b>MBB</b> Messerschmitt Bölkow Blohm
<b>BK2-2D</b> second 2D benchmark problem	<b>MMC</b> moving morphable component
<b>BK3D</b> 3D benchmark problem	<b>MMV</b> moving morphable void
<b>B-spline</b> basis spline	<b>ND</b> Neumann-Dirichlet
<b>BC</b> boundary condition	<b>NLPP</b> non-linear programming problem
<b>BESO</b> bi-directional evolutionary structural optimisation	<b>NURBS</b> non-uniform rational basis spline
<b>CAD</b> computer aided design	<b>SANTO</b> SIMP and NURBS for topology optimisation
<b>CNLPP</b> constrained non-linear programming problem	<b>SIMP</b> solid isotropic material with penalisation
<b>CP</b> control point	<b>TO</b> topology optimisation
<b>DOF</b> degree of freedom	<b>TPE</b> total potential energy
<b>ESO</b> evolutionary structural optimisation	<b>TV</b> topological variable
<b>FE</b> finite element	<b>WAFD</b> work of applied forces and displacements
<b>GCMMA</b> globally-convergent method of moving asymptotes	

## 1. Introduction

Nowadays topology optimisation (TO) methods are increasingly used in several industrial sectors during the preliminary design phase of a product/system. TO is, indeed, knowing a new “era” mainly because of the development of modern additive manufacturing (AM) technologies, which can be exploited to manufacture products of complex shapes. Moreover, during the last 30 years, TO has gained an increasing attention to such an extent that, today, it constitutes a widespread research topic in different fields of study.

The goal of TO is to determine the optimal distribution of the material, within a prescribed domain, to minimise a given merit function, while satisfying a set of design requirements. Among the different TO methods available in the literature, the solid isotropic material with penalisation (SIMP) approach [1, 2], and the level set method (LSM) [3–6], are, undoubtedly, the most popular methodologies.

In the context of the SIMP approach [1, 2], the goal is to find the optimal distribution of a fictitious, heterogeneous material by introducing a pseudo-density field,  $\rho(x) \in [0, 1]$ , which affects, via a penalisation law, the stiffness tensor of the elements constituting the finite element (FE) model.

In the framework of the LSM, the FE model is used solely to evaluate the physical responses involved into the problem formulation. The topological descriptor is a level-set function, whose sign is conventionally associated to solid or void zones, while the zero value represents the boundary of the optimised structure [6]. A detailed discussion of the LSM for TO is available in [3–6].

Further TO methods available in the literature include: the evolutionary structural optimisation (ESO) method [7] and its extension, i.e., the bi-directional evolutionary structural optimisation (BESO) method [8]. The ESO method is based on the combination of a metaheuristic algorithm and the FE method, whilst the BESO method is a generalisation of the former, which includes operators able to produce mesh-independent results (without

checker-board pattern) and a sensitivity number averaging method, which allows avoiding convergence issues [9, 10].

Among the most recent TO methods allowing for both a design variables count reduction during optimisation and an explicit representation of the boundary of the optimised topology it is worth to mention the moving morphable component (MMC) approach [11] and its dual counterpart, i.e., the moving morphable void (MMV) method [12]. An efficient and versatile method belonging to this class is the SIMP method reformulated in the framework of non-uniform rational basis spline (NURBS) hyper-surfaces [13–21]. Unlike classical density-based TO approaches [2], the NURBS-based SIMP method separates the pseudo-density field, describing the topology of the continuum, from the mesh of the FE model. More precisely, for general 3D problems, a 4D NURBS hyper-surface is used as a topological descriptor, whilst for 2D problems a standard 3D NURBS surface is employed. In this way, the topological descriptor, i.e., the pseudo-density field, relies on a purely geometric entity.

In the framework of the NURBS-based SIMP method, the computer aided design (CAD) reconstruction phase of the optimised topology becomes a trivial task [22, 23] because the topology boundary is available (at each iteration of the optimisation process) in a CAD-compatible format (thanks to the use of NURBS entities). Moreover, some fundamental properties of the NURBS basis functions, like the local support property, can be conveniently exploited to determine the gradient of the physical responses with respect to the topological variables, i.e., the pseudo-density evaluated at control points (CPs) and the related weights. Indeed, as discussed in [16, 17], NURBS entities allow for handling in the most efficient way the design requirements of geometrical nature (like minimum and maximum length scale requirements) during the optimisation process.

Regardless of the adopted TO method, it is a well-known fact that the most studied problem in the literature is the one dealing with the maximisation of the structural stiffness subject to a design requirement on the total volume/mass [2]. It is noteworthy that, in the vast majority of cases [1, 2, 4, 5, 7, 8, 10–14], a combination of non-zero boundary conditions (BCs) of the Neumann type (i.e., on generalised forces) and null BCs of the Dirichlet type (i.e., on generalised displacements) are imposed on the nodes belonging to the boundary. In such cases, the work of applied forces and displacements (WAFD) can be adopted as a measure of the structural stiffness.

Nevertheless, the WAFD cannot be considered as a measure of the structural stiffness when non-zero Dirichlet’s BCs are considered. To the best of the author’s knowledge, the effect of mixed non-zero Neumann-Dirichlet (ND) BCs on the structural maximisation problem formulation has been investigated only by few authors [24–27]. In [24], the authors studied the influence of non-zero Dirichlet’s type BCs on both minimum compliance and maximum strength problems. However, the merit function used as a measure of the compliance in [24] was the total elastic energy (defined as twice the strain energy) of the continuum which equals the WAFD (under static equilibrium condition). The authors noticed that the two problem formulations lead to different design and the optimised topologies obtained in both cases are not characterised by a uniform distribution of the strain energy density.

In [25], Niu *et al.* proposed a new formulation of structural maximisation problems under non-zero mixed BCs by introducing a new functional obtained as a linear combination of the WAFD and of the work done by reaction forces at nodes where non-zero Dirichlet’s BCs are applied. They provided a proof to determine the gradient of this functional, by showing that it is equal to the gradient of the compliance in the standard case of non-zero Neumann’s BCs and zero Dirichlet’s BCs. Moreover, they conducted a sensitivity analysis

of the optimised topology to the applied non-zero displacement.

Later, and independently, Klarbring and Strömberg [26] and Barbarosie and Lopes [27] proved that the formulation of the structural maximisation problem proposed by [25] can be related, from a calculus of variations standpoint, to the minimisation of a merit function proportional to the total potential energy (TPE) of the continuum. In particular, Klarbring and Strömberg [26] formalised this concept by using a notation related to the discrete algebraic formulation of the FE method, by confirming the results found in [25]. On the other hand, Barbarosie and Lopes [27] proposed a formulation (referred to as *generalised compliance*) making use of the formalism of variational mechanics. They highlighted, by using a low-resolution density-based TO method, that the results obtained by minimising the generalised compliance are different from those obtained minimising the WAFD.

This work aims to shed a light on the influence of mixed non-zero BCs on the structural stiffness maximisation problem of anisotropic continua. Particularly, three theoretical/numerical aspects are discussed in this study.

Firstly, a proof simpler than the one proposed in [25] is provided to determine the gradient of the merit function related to the TPE.

Secondly, it is shown that, under mixed non-zero ND BCs, the optimisation problem making use of the TPE as structural stiffness descriptor is self-adjoint while the one making use of the WAFD as merit function is not self-adjoint.

Finally, three sensitivity analyses are conducted for both problem formulations (i.e., minimisation of the WAFD and minimisation of the functional related to the TPE). The first one aims to assess the influence of the elastic symmetry type of the continuum on the optimised topology. The second one aims to investigate the influence of the non-zero Dirichlet's type BCs on the solution. The last one aims to determine the influence of the design requirement on the volume fraction on the optimised solution.

A large campaign of numerical tests is conducted on both 2D and 3D benchmark problems: results highlight that, depending on the elastic symmetry type of the continuum and on the value of the constraint on the volume fraction, the optimal topologies resulting from the two problem formulations can be the same.

The remainder of the paper is as follows. The fundamentals of NURBS hyper-surfaces are briefly recalled in Sec. 2. The main features of the NURBS-based SIMP method and the two problem formulations involving the WAFD and the TPE as merit functions, respectively, are presented in Sec. 3. The numerical results are presented and discussed in Sec. 4, whilst Sec. 5 ends the paper with meaningful conclusions and prospects.

*Notation.* Upper-case bold letters and symbols are used to indicate tensors and matrices, while lower-case bold letters and symbols indicate column vectors.  $\#\mathcal{S}$  denotes the cardinality of the generic set  $\mathcal{S}$ .

## 2. NURBS hyper-surfaces

A NURBS hyper-surface is a polynomial-based function, defined as  $\mathbf{h} : \mathbb{R}^N \rightarrow \mathbb{R}^D$ , where  $N$  is the dimension of the parametric space, whilst  $D$  is the dimension of the co-domain. The formula of a NURBS hyper-surface reads:

$$\mathbf{h}(\zeta_1, \dots, \zeta_N) := \sum_{i_1=0}^{n_1} \cdots \sum_{i_N=0}^{n_N} R_{i_1 \dots i_N}(\zeta_1, \dots, \zeta_N) \mathbf{y}_{i_1, \dots, i_N}, \quad (1)$$

where  $R_{i_1 \dots i_N}(\zeta_1, \dots, \zeta_N)$  are the piece-wise rational basis functions, which are related to the standard Bernstein's polynomials  $N_{i_k, p_k}(\zeta_k)$ , ( $k = 1, \dots, N$ ) by means of the relationship:

$$R_{i_1 \dots i_N} := \frac{\omega_{i_1 \dots i_N} \prod_{k=1}^N N_{i_k, p_k}(\zeta_k)}{\sum_{j_1=0}^{n_1} \dots \sum_{j_N=0}^{n_N} \left[ \omega_{j_1 \dots j_N} \prod_{k=1}^N N_{j_k, p_k}(\zeta_k) \right]}. \quad (2)$$

In Eqs. (1) and (2),  $\mathbf{h}(\zeta_1, \dots, \zeta_N)$  is a  $D$ -dimension vector-valued rational function,  $\zeta_k \in [0, 1]$  is the  $k$ -th dimensionless coordinate (or parametric coordinate), whilst  $\mathbf{y}_{i_1, \dots, i_N} \in \mathbb{R}^D$  are the control points (CPs) coordinates, while  $n_j \in \mathbb{N}$  and  $p_j \in \mathbb{N} \cup 0$  ( $j = 1, \dots, N$ ) are the number of CPs and the basis functions degree, respectively, along the  $\zeta_j$  parametric direction. The  $j$ -th CP coordinate  $y_{i_1, \dots, i_N}^{(j)}$  is stored in the array  $\mathbf{Y}^{(j)} \in \mathbb{R}^{(n_1+1) \times \dots \times (n_N+1)}$ ,  $j = 1, \dots, D$ . The explicit expression of CPs coordinates is:

$$\mathbf{Y}_{i_1, \dots, i_N}^T = \{y_{i_1, \dots, i_N}^{(1)}, \dots, y_{i_1, \dots, i_N}^{(D)}\}. \quad (3)$$

The CPs layout is referred to as *control hyper-net* [28]. The generic CP affects the shape of the NURBS entity by means of its coordinates. The overall number of CPs constituting the hyper-net is:

$$n_{\text{CP}} := \prod_{i=1}^N (n_i + 1). \quad (4)$$

In Eq. (2), a weight  $\omega_{i_1 \dots i_N}$  is associated to the generic CP. The higher the weight the more the NURBS entity is attracted towards the associated CP. For each parametric direction  $\zeta_k$ , the NURBS blending functions  $N_{i_k, p_k}(\zeta_k)$  appearing in Eq. (2) can be defined recursively as:

$$N_{i_k, 0}(\zeta_k) := \begin{cases} 1, & \text{if } v_{i_k}^{(k)} \leq \zeta_k < v_{i_k+1}^{(k)}, \\ 0, & \text{otherwise,} \end{cases} \quad (5)$$

$$N_{i_k, q}(\zeta_k) = \frac{\zeta_k - v_{i_k}^{(k)}}{v_{i_k+q}^{(k)} - v_{i_k}^{(k)}} N_{i_k, q-1}(\zeta_k) + \frac{v_{i_k+q+1}^{(k)} - \zeta_k}{v_{i_k+q+1}^{(k)} - v_{i_k+1}^{(k)}} N_{i_k+1, q-1}(\zeta_k), \quad q = 1, \dots, p_k, \quad k = 1, \dots, N, \quad (6)$$

where each constitutive blending function is defined on the knot vector:

$$\mathbf{v}_{(k)}^T = \underbrace{\{0, \dots, 0\}}_{p_k+1}, v_{p_k+1}^{(k)}, \dots, v_{m_k-p_k-1}^{(k)}, \underbrace{\{1, \dots, 1\}}_{p_k+1}, \quad \mathbf{v}_{(k)} \in \mathbb{R}^{m_k+1}, \quad k = 1, \dots, N, \quad (7)$$

with:

$$m_k = n_k + p_k + 1. \quad (8)$$

The NURBS blending functions are characterised by several interesting properties: the interested reader is addressed to [28] for more details on the topic. Here, only the *local support property* is recalled because it is exploited in the context of the NURBS-based

SIMP method [13, 14]:

$$R_{i_1 \dots i_N}(\zeta_1, \dots, \zeta_N) \neq 0, \text{ if } (\zeta_1, \dots, \zeta_N) \in \left[ v_{i_1}^{(1)}, v_{i_1+p_1+1}^{(1)} \right] \times \dots \times \left[ v_{i_N}^{(N)}, v_{i_N+p_N+1}^{(N)} \right]. \quad (9)$$

Eq. (9) means that each CP (and the respective weight) affects only a precise zone of the parametric space, which is denoted as *local support*.

### 3. The NURBS-based SIMP method

A detailed description of the mathematical background of the NURBS-based SIMP method is available in [13, 14]. The main features of the approach are briefly described here only for 3D TO problems.

#### 3.1. Design variables

Consider the compact Euclidean space  $\mathcal{D} \subset \mathbb{R}^3$ , defining the design domain in a Cartesian orthogonal frame  $O(x_1, x_2, x_3)$ :

$$\mathcal{D} := \{ \mathbf{x}^T = (x_1, x_2, x_3) \in \mathbb{R}^3 : x_j \in [0, L_j], j = 1, 2, 3 \}, \quad (10)$$

where  $L_j$ , is the characteristic length of the domain defined along  $x_j$  axis. In the SIMP approach the *material domain*  $\Omega \subseteq \mathcal{D}$  is identified by means of the pseudo-density function  $\rho(\mathbf{x}) \in [0, 1]$  for  $\mathbf{x} \in \mathcal{D}$ :  $\rho(\mathbf{x}) = 0$  means absence of material, whilst  $\rho(\mathbf{x}) = 1$  implies presence of material.

In the context of the NURBS-based SIMP method, the topological variable (TV), i.e., the pseudo-density field, for a problem of dimension  $D$  is represented by means of a NURBS entity of dimension  $D + 1$ . Therefore, if a 3D TO problem is considered, a 4D NURBS hyper-surface is needed to describe the part topology [14]. The first three coordinates of the NURBS entity correspond to the Cartesian coordinates defining the domain, while the last coordinate is the pseudo-density field that reads:

$$\rho(\zeta_1, \zeta_2, \zeta_3) = \sum_{i_1=0}^{n_1} \sum_{i_2=0}^{n_2} \sum_{i_3=0}^{n_3} R_{i_1 i_2 i_3}(\zeta_1, \zeta_2, \zeta_3) \rho_{i_1 i_2 i_3}. \quad (11)$$

In Eq. (11),  $\rho_{i_1 i_2 i_3}$  is the value of the pseudo-density at the generic CP, i.e., the fourth coordinate of the vector  $\mathbf{h}$  in Eq. (1), while  $R_{i_1 i_2 i_3}$  is the generic rational basis function of Eq. (2).

The dimensionless parameters  $\zeta_j$  can be defined as:

$$\zeta_j := \frac{x_j}{L_j}, j = 1, 2, 3. \quad (12)$$

Among the parameters involved in the definition of the NURBS entity, only the pseudo-density at CPs and the associated weights are included in the design variable vectors  $\boldsymbol{\xi}_1$  and  $\boldsymbol{\xi}_2$ , which are defined as:

$$\boldsymbol{\xi}_1^T := (\rho_{000}, \dots, \rho_{n_1 n_2 n_3}), \boldsymbol{\xi}_2^T := (\omega_{000}, \dots, \omega_{n_1 n_2 n_3}), \boldsymbol{\xi}_1, \boldsymbol{\xi}_2 \in \mathbb{R}^{n_{\text{CP}}}, \quad (13)$$

accordingly, the number of design variables is, at most,  $n_{\text{var}} = 2n_{\text{CP}}$ .

The other parameters tuning the shape of the NURBS entity, i.e., degrees, knot-vector components and number of CPs, are pre-defined at the beginning of the optimisation process. For a deeper insight in the NURBS-based SIMP method the reader is addressed to [13, 14].

### 3.2. Objective function

Consider the static equilibrium of the FE model in the most general case of mixed non-zero ND BCs:

$$\hat{\mathbf{K}}\hat{\mathbf{u}} = \hat{\mathbf{f}}, \quad \hat{\mathbf{u}}, \hat{\mathbf{f}} \in \mathbb{R}^{\hat{N}_{\text{DOF}}}, \quad \hat{\mathbf{K}} \in \mathbb{R}^{\hat{N}_{\text{DOF}} \times \hat{N}_{\text{DOF}}}, \quad (14)$$

where  $\hat{N}_{\text{DOF}}$  is the overall number of degrees of freedom (DOFs) before the application of BCs,  $\hat{\mathbf{K}}$  is the non-reduced (singular) stiffness matrix of the FE model, while  $\hat{\mathbf{f}}$  and  $\hat{\mathbf{u}}$  are the non-reduced vectors of the external generalised nodal forces and displacements, respectively. Consider, now, the following definition:

**Definition 3.1.** Let  $\hat{\mathfrak{M}} \in \mathbb{R}^{m \times n}$  be a generic rectangular matrix and  $\mathcal{R} \subset \{i \mid 1 \leq i \leq m\}$  and  $\mathcal{C} \subset \{j \mid 1 \leq j \leq n\}$  two sets of positive natural numbers. The operator  $\mathfrak{R} := \mathfrak{R}(\hat{\mathfrak{M}}, \mathcal{R}, \mathcal{C})$  returns the matrix  $\mathfrak{M}$  obtained by deleting the  $i$ -th row and the  $j$ -th column from  $\hat{\mathfrak{M}}$ ,  $\forall i \in \mathcal{R}$  and  $\forall j \in \mathcal{C}$ . Similarly, given  $\hat{\mathbf{v}} \in \mathbb{R}^n$ ,  $\mathbf{v} := \mathfrak{R}(\hat{\mathbf{v}}, \mathcal{R})$  denotes the vector obtained by suppressing the  $i$ -th row of  $\hat{\mathbf{v}}$ ,  $\forall i \in \mathcal{R}$ .

Let  $\mathcal{I}_U \subset \{i \mid 1 \leq i \leq \hat{N}_{\text{DOF}}\}$  and  $\mathcal{I}_{\text{BC}} \subset \{i \mid 1 \leq i \leq \hat{N}_{\text{DOF}}\}$  be two generic sets of indices such that:  $\mathcal{I}_U \cap \mathcal{I}_{\text{BC}} = \emptyset$ ,  $\#\mathcal{I}_U = N_{\text{DOF}}$ ,  $\#\mathcal{I}_{\text{BC}} = N_{\text{BC}}$  and  $N_{\text{DOF}} + N_{\text{BC}} = \hat{N}_{\text{DOF}}$  (i.e.,  $N_{\text{BC}}$  is the number of DOFs where displacements are imposed, whilst  $N_{\text{DOF}}$  is the number of unknown DOFs). By applying Def. 3.1 to Eq. (14), one gets

$$\begin{bmatrix} \mathbf{K} & \mathbf{K}_{\text{BC}} \\ \mathbf{K}_{\text{BC}}^T & \tilde{\mathbf{K}} \end{bmatrix} \begin{Bmatrix} \mathbf{u} \\ \mathbf{u}_{\text{BC}} \end{Bmatrix} = \begin{Bmatrix} \mathbf{f} \\ \mathbf{r} \end{Bmatrix}, \quad (15)$$

with:

$$\begin{aligned} \mathbf{u} &:= \mathfrak{R}(\hat{\mathbf{u}}, \mathcal{I}_{\text{BC}}), \quad \mathbf{f} := \mathfrak{R}(\hat{\mathbf{f}}, \mathcal{I}_{\text{BC}}) \\ \mathbf{u}_{\text{BC}} &:= \mathfrak{R}(\hat{\mathbf{u}}, \mathcal{I}_U), \quad \mathbf{r} := \mathfrak{R}(\hat{\mathbf{f}}, \mathcal{I}_U), \\ \mathbf{K} &:= \mathfrak{R}(\hat{\mathbf{K}}, \mathcal{I}_{\text{BC}}, \mathcal{I}_{\text{BC}}), \quad \mathbf{K}_{\text{BC}} := \mathfrak{R}(\hat{\mathbf{K}}, \mathcal{I}_{\text{BC}}, \mathcal{I}_U), \quad \tilde{\mathbf{K}} := \mathfrak{R}(\hat{\mathbf{K}}, \mathcal{I}_U, \mathcal{I}_U), \\ \mathbf{u}, \mathbf{f} &\in \mathbb{R}^{N_{\text{DOF}}}, \quad \mathbf{u}_{\text{BC}}, \mathbf{r} \in \mathbb{R}^{N_{\text{BC}}}, \\ \mathbf{K} &\in \mathbb{R}^{N_{\text{DOF}} \times N_{\text{DOF}}}, \quad \mathbf{K}_{\text{BC}} \in \mathbb{R}^{N_{\text{DOF}} \times N_{\text{BC}}}, \quad \tilde{\mathbf{K}} \in \mathbb{R}^{N_{\text{BC}} \times N_{\text{BC}}}. \end{aligned} \quad (16)$$

In Eq. (15),  $\mathbf{u}$  and  $\mathbf{u}_{\text{BC}}$  are the unknown and imposed vectors of generalised displacements, respectively;  $\mathbf{f}$  is the vector of generalised external nodal forces, whilst  $\mathbf{r}$  is the vector of (unknown) generalised nodal reactions on the nodes where BCs on generalised displacements are imposed.  $\mathbf{K}$ ,  $\mathbf{K}_{\text{BC}}$  and  $\tilde{\mathbf{K}}$  are the stiffness matrices of the FE model after applying BCs.

In the context of the SIMP approach, the density field of Eq. (11) affects the element

stiffness matrix and, accordingly, the global stiffness matrix of the FE model as follows:

$$\begin{aligned}\hat{\mathbf{K}} &:= \sum_{e=1}^{N_e} \rho_e^\alpha \hat{\mathbf{L}}_e^T \mathbf{K}_e^0 \hat{\mathbf{L}}_e = \sum_{e=1}^{N_e} \hat{\mathbf{L}}_e^T \mathbf{K}_e \hat{\mathbf{L}}_e, \\ \mathbf{K}_e^0, \mathbf{K}_e &\in \mathbb{R}^{N_{\text{DOF}}^e \times N_{\text{DOF}}^e}, \quad \hat{\mathbf{L}}_e \in \mathbb{R}^{N_{\text{DOF}}^e \times \hat{N}_{\text{DOF}}},\end{aligned}\tag{17}$$

where  $\rho_e$  is the fictitious density of Eq. (11) computed at the centroid of the generic element  $e$ , whilst  $\alpha \geq 1$  is a suitable parameter used to penalise the intermediate densities between 0 and 1, in agreement with the classic SIMP approach ( $\alpha = 3$  in this study).  $N_e$  is the total number of elements and  $N_{\text{DOF}}^e$  is the number of DOFs of the generic element. In Eq. (17),  $\mathbf{K}_e^0$  and  $\mathbf{K}_e$  are the non-penalised and the penalised stiffness matrices of element  $e$ , expressed in the global reference frame of the FE model, whilst  $\hat{\mathbf{L}}_e$  is the connectivity matrix of element  $e$  relating the DOFs at the element-level to their counterparts at the structure-level:

$$\mathbf{u}_e = \hat{\mathbf{L}}_e \hat{\mathbf{u}},\tag{18}$$

where  $\mathbf{u}_e \in \mathbb{R}^{N_{\text{DOF}}^e}$  is the vector of nodal displacements for element  $e$ .

The physical responses functions related to the design requirements considered in this study are presented in the following. Two different merit functions (related to just as many requirements) are considered. The first one is the WAFD which reads:

$$\mathcal{W}(\boldsymbol{\xi}_1, \boldsymbol{\xi}_2) := \mathbf{f}^T \mathbf{u} + \mathbf{u}_{\text{BC}}^T \mathbf{r}.\tag{19}$$

The second one is the so-called generalised compliance [26, 27], which depends upon the TPE of the continuum  $\Pi$  as follows:

$$\mathcal{C}(\boldsymbol{\xi}_1, \boldsymbol{\xi}_2) := -2\Pi(\boldsymbol{\xi}_1, \boldsymbol{\xi}_2),\tag{20}$$

where the TPE is defined as

$$\Pi(\boldsymbol{\xi}_1, \boldsymbol{\xi}_2) := \frac{1}{2} \hat{\mathbf{u}}^T \hat{\mathbf{K}} \hat{\mathbf{u}} - \mathbf{f}^T \mathbf{u}.\tag{21}$$

By injecting Eq. (15) in Eq. (21) and, subsequently, Eq. (21) in Eq. (20), the generalised compliance reads:

$$\mathcal{C}(\boldsymbol{\xi}_1, \boldsymbol{\xi}_2) = \mathbf{f}^T \mathbf{u} - \mathbf{u}_{\text{BC}}^T \mathbf{r}.\tag{22}$$

The physical meaning of the generalised compliance in the form of Eq. (22) is intuitively clear: a stiff structure should react to the applied loads by having small displacements and to the applied displacements by having large reaction forces. Conversely, this is not the case when the WAFD of Eq. (19) is used as objective function under mixed inhomogeneous BCs.

Inasmuch as the solution search for the TO problem is carried out by means of a suitable deterministic algorithm, the derivation of the formal expression of the gradient of the objective function with respect to the TVs (and of the constraint function too) is needed to speed up the iterations. To this end, consider the following propositions.

**Proposition 3.1.** *Consider a deformable continuum subject to given external loads and*

displacements. If the imposed loads and displacements are independent from the pseudo-density field, the gradient of the WAFD reads:

$$\frac{\partial \mathcal{W}}{\partial \xi_{i\tau}} = \sum_{e \in \mathcal{S}_\tau} \frac{\alpha}{\rho_e} \frac{\partial \rho_e}{\partial \xi_{i\tau}} (w_e - 2\mathbf{u}_{e0}^T \mathbf{f}_e), \quad i = 1, 2, \quad \tau = 1, \dots, n_{\text{CP}}. \quad (23)$$

where the internal work of the generic element  $e$ , i.e.,  $w_e$ , is defined as

$$w_e := \mathbf{u}_e^T \mathbf{K}_e \mathbf{u}_e, \quad (24)$$

whilst  $\mathbf{u}_{e0}$  and  $\mathbf{f}_e$  can be obtained from the following relations

$$\mathbf{u}_{e0} = \mathfrak{R}(\hat{\mathbf{L}}_e, \emptyset, \mathcal{I}_{\text{BC}}) \mathbf{u}_0 = \mathbf{L}_e \mathbf{u}_0, \quad (25)$$

$$\mathbf{f}_e = \rho_e^\alpha \mathbf{K}_e^0 \mathbf{u}_e = \mathbf{K}_e \mathbf{u}_e. \quad (26)$$

A proof of proposition 3.1 is provided in Appendix A.

**Remark 3.1.** The vector of nodal displacements  $\mathbf{u}_0$  appearing in Eq. (25) is the solution of Eq. (15) when BCs of Dirichlet's type are null, i.e.,  $\mathbf{u}_{\text{BC}} = \mathbf{0}$ . In this case the equilibrium equation simplifies to:

$$\mathbf{K} \mathbf{u}_0 = \mathbf{f}. \quad (27)$$

**Remark 3.2.** The WAFD is not a self-adjoint functional because to assess its gradient the following adjoint vector must be introduced:

$$\boldsymbol{\eta} = \mathbf{u} - 2\mathbf{u}_0, \quad (28)$$

which requires the resolution of the auxiliary system of Eq. (27). All the details about the adjoint system of which  $\boldsymbol{\eta}$  is the solution are provided in Appendix A.

**Remark 3.3.** In Eq. (23), the linear index  $\tau$  has been introduced for the sake of compactness. The relation between  $\tau$  and  $i_j$ , ( $j = 1, 2, 3$ ) is:

$$\tau := 1 + i_1 + i_2(n_1 + 1) + i_3(n_1 + 1)(n_2 + 1). \quad (29)$$

Moreover, in Eq. (23), the quantity  $\mathcal{S}_\tau$  is the discretised version of the local support of Eq. (9), while  $\frac{\partial \rho_e}{\partial \xi_{i\tau}}$  reads:

$$\frac{\partial \rho_e}{\partial \xi_{i\tau}} = \begin{cases} R_{\tau e}, & \text{if } i = 1, \\ \frac{R_{\tau e}}{\xi_{2\tau}} (\xi_{1\tau} - \rho_e), & \text{if } i = 2. \end{cases} \quad (30)$$

The scalar quantity  $R_{\tau e}$  appearing in Eq. (30) is the NURBS rational basis function of Eq. (2) evaluated at the element centroid.

**Proposition 3.2.** *Under the same hypotheses of Prop. 3.1, the gradient of the generalised compliance reads:*

$$\frac{\partial \mathcal{C}}{\partial \xi_{i\tau}} = - \sum_{e \in \mathcal{S}_\tau} \frac{\alpha}{\rho_e} \frac{\partial \rho_e}{\partial \xi_{i\tau}} w_e, \quad i = 1, 2, \quad \tau = 1, \dots, n_{\text{CP}}. \quad (31)$$

A proof of proposition 3.2, simpler than the one presented by [25], is provided in Appendix B.

### 3.3. Constraint functions

Two design requirements are considered in this study. The first one deals with the lightness of the structure and is formulated in terms of a constraint on the overall volume of the structure  $V$ :

$$V = \sum_{e=1}^{N_e} \rho_e V_e, \quad (32)$$

where  $V_e$  is the volume of the generic element. By differentiating Eq. (32) one obtains:

$$\frac{\partial V}{\partial \xi_{i\tau}} = \sum_{e \in \mathcal{S}_\tau} V_e \frac{\partial \rho_e}{\partial \xi_{i\tau}}, \quad i = 1, 2, \quad \tau = 1, \dots, n_{\text{CP}}. \quad (33)$$

Therefore the lightness requirement can be formulated as:

$$g_1(\boldsymbol{\xi}_1, \boldsymbol{\xi}_2) := \frac{V}{V_{\text{ref}}} - \gamma \leq 0, \quad (34)$$

where  $V_{\text{ref}}$  is a reference value of the volume, whilst  $\gamma$  is the imposed volume fraction.

The second requirement deals with the manufacturing constraint on the minimum thickness that can be fabricated through the selected manufacturing process. This requirement is formulated as minimum length scale (or minimum member size) constraint as:

$$g_2(\boldsymbol{\xi}_1, \boldsymbol{\xi}_2) := 1 - \frac{d_{\text{min}}}{d_{\text{MP}}} \leq 0. \quad (35)$$

In Eq. (35),  $d_{\text{min}}$  is the minimum length scale of the topology, while  $d_{\text{MP}}$  is the minimum dimension that can be obtained through the considered manufacturing process.

**Remark 3.4.** *As discussed in [16], the main advantage of the NURBS-based SIMP method is in the handling of the geometric constraints imposed on the TV. In particular, since the pseudo-density field describing the topology of the continuum is described by means of a NURBS hyper-surface, it is possible to properly set the integer parameters (i.e., number of CPs  $n_{\text{CP}}$  and basis functions degree  $p_j$  along each parametric direction) governing its shape to automatically satisfy the minimum length scale requirement, without introducing an explicit optimisation constraint in the problem formulation. Therefore, in the following, the manufacturing requirement of Eq. (35) will be controlled through this feature.*

**Remark 3.5.** *As discussed in [16], unlike the classical SIMP method, the minimum member size requirement, which can be met by properly tuning the value of the integer parameters involved in the definition of the NURBS entity does not depend upon the size of the*

elements composing the mesh. This means that an eventual mesh refinement has an impact only on the value of the structural responses (displacements, strains, stresses, etc.), but not on the minimum member size of the topology.

### 3.4. Problem formulation

Two different problem formulations are considered in this work, depending on the considered objective function, i.e., the work of applied forces and displacements and the generalised compliance. In each case, the optimisation problem is formulated in the form of a non-linear programming problem (NLPP). The two formulations read:

$$\min_{\boldsymbol{\xi}_1, \boldsymbol{\xi}_2} \frac{\mathcal{W}(\boldsymbol{\xi}_1, \boldsymbol{\xi}_2)}{\mathcal{W}_{\text{ref}}}, \text{ subject to : } \begin{cases} \hat{\mathbf{K}}\hat{\mathbf{u}} = \hat{\mathbf{f}}, \\ g_1(\boldsymbol{\xi}_1, \boldsymbol{\xi}_2) \leq 0, \\ \boldsymbol{\xi}_{1\tau} \in [\rho_{\min}, \rho_{\max}], \quad \boldsymbol{\xi}_{2\tau} \in [\omega_{\min}, \omega_{\max}], \\ k = 1, \dots, n_{\text{CP}}, \end{cases} \quad (36)$$

$$\min_{\boldsymbol{\xi}_1, \boldsymbol{\xi}_2} \frac{\mathcal{C}(\boldsymbol{\xi}_1, \boldsymbol{\xi}_2)}{\mathcal{C}_{\text{ref}}}, \text{ subject to : } \begin{cases} \hat{\mathbf{K}}\hat{\mathbf{u}} = \hat{\mathbf{f}}, \\ g_1(\boldsymbol{\xi}_1, \boldsymbol{\xi}_2) \leq 0, \\ \boldsymbol{\xi}_{1\tau} \in [\rho_{\min}, \rho_{\max}], \quad \boldsymbol{\xi}_{2\tau} \in [\omega_{\min}, \omega_{\max}], \\ k = 1, \dots, n_{\text{CP}}. \end{cases} \quad (37)$$

In Eqs. (36) and (37),  $\mathcal{W}_{\text{ref}}$  and  $\mathcal{C}_{\text{ref}}$  are the reference value of the WAFD and of the compliance of the structure, respectively, whilst  $\rho_{\min}$  and  $\rho_{\max}$  are lower and upper bounds of the pseudo-density at each CP, and  $\omega_{\min}$  and  $\omega_{\max}$  are the bounds on the weights. Of course, the lower bound of the pseudo-density must be strictly positive to prevent any singularity for the solution of the equilibrium problem. The overall number of design variables of problems (36) and (37) is equal to  $n_{\text{var}} = 2n_{\text{CP}}$ .

## 4. Numerical results

The effectiveness of the proposed method is illustrated on 2D and 3D benchmark problems taken from the literature [25, 27]. For each case, the pseudo-density field and the optimum topology are shown. The results presented here are obtained through the code SANTO (SIMP and NURBS for topology optimisation) developed at the I2M laboratory in Bordeaux [13, 14]. SANTO is coded in the Python<sup>®</sup> environment and can be interfaced with any FE code. In this study, the FE code ANSYS<sup>®</sup> is used to generate the FE model of each benchmark problem and to assess the structural responses, i.e. the WAFD and the generalised compliance.

Moreover, the globally-convergent method of moving asymptotes (GCMMA) algorithm [29] is employed to carry out the solution search for the CNLPPs of Eqs. (36) and (37). The parameters governing its behaviour are listed in Table 1.

Regarding the campaign of numerical simulations, the following aspects are investigated:

1. The influence of the geometric entity, i.e., basis spline (B-spline) or NURBS, used to describe the TV on the optimised solution (only for 2D problems for the sake of brevity);

Table 1: GCMMA algorithm parameters

Parameter	Value
<i>move</i>	0.1
<i>albefa</i>	0.1
Stop Criterion	Value
Maximum n. of function evaluations	$100 \times n_{\text{var}}$
Maximum n. of iterations	500
Tolerance on objective function	$10^{-6}$
Tolerance on constraints	$10^{-6}$
Tolerance on input variables change	$10^{-6}$
Tolerance on Karush–Kuhn–Tucker norm	$10^{-6}$

2. The influence of mixed non-zero BC on the optimised topology (for 2D and 3D problems);
3. The influence of the elastic symmetry group on the optimised solution (for both 2D and 3D problems);
4. The influence of the constraint on the volume fraction on the optimised solution (only for 2D problems for the sake of brevity).

**Remark 4.1.** *The reference values of both WAFD and generalised compliance, i.e.,  $\mathcal{W}_{\text{ref}}$  and  $\mathcal{C}_{\text{ref}}$ , respectively, are those characterising the starting guess. Moreover, the reference volume  $V_{\text{ref}}$  is the volume of the overall design domain of dimension  $D = 2, 3$ .*

**Remark 4.2.** *For each CNLPP, lower and upper bounds of design variables are set as:  $\rho_{\min} = 10^{-3}$ ,  $\rho_{\max} = 1$ ;  $\omega_{\min} = 0.5$ ,  $\omega_{\max} = 10$ . It is noteworthy that the non-trivial components of the knot-vectors in Eq. (7) are evenly distributed in the interval  $[0, 1]$  for each benchmark problem.*

**Remark 4.3.** *All the analyses presented in the following of this document have been performed on a work-station with an Intel Xeon E5-2697v2 processor (2.70–3.50 GHz) and four cores dedicated to the optimisation calculations. The highest computational time occurs in the 3D case, which required about 1h to find the local feasible minimiser.*

#### 4.1. 2D benchmark problems

The first 2D benchmark problem (BK1-2D), taken from [25], deals with the well-known Messerschmitt Bölkow Blohm (MBB) beam submitted to mixed non-zero BCs, as shown in Fig. 1a. The geometrical parameters defining the design domain are:  $L_1 = 300$  mm and  $L_2 = 100$  mm. The FE model is made of  $N_e = 120 \times 40$  PLANE182 elements (i.e. plane elements, with four nodes and two DOFs per node, plane stress hypothesis with unit thickness) and it subjected to the following BCs:

- The node located  $(x_1, x_2) = (0, 0)$  is clamped ( $u_1 = u_2 = 0$ );
- $u_1 = \delta_1$  and  $u_2 = 0$  are set on the node located  $(x_1, x_2) = (L_1, 0)$ ; the displacement  $\delta_1$  varies in the interval  $[-40, 40]$  mm with a step of 10 mm;
- $F_2 = -1$  N is applied at the node located at  $(x_1, x_2) = (\frac{L_1}{2}, 0)$ .

The second 2D benchmark problem (BK2-2D), taken from [27] and illustrated in Fig. 1b, is characterised by the same geometrical parameters and the same mesh of BK1-2D. The applied BCs are:

- The nodes located at  $(x_1, x_2) = (0, 0)$  and  $(x_1, x_2) = (L_1, 0)$  are clamped ( $u_1 = u_2 = 0$ );
- $u_2 = \delta_2 = -8$  mm is set on the node located  $(x_1, x_2) = (\frac{2}{3}L_1, 0)$ ;
- $F_2 = -1$  N is applied at the node located at  $(x_1, x_2) = (\frac{L_1}{3}, 0)$ .

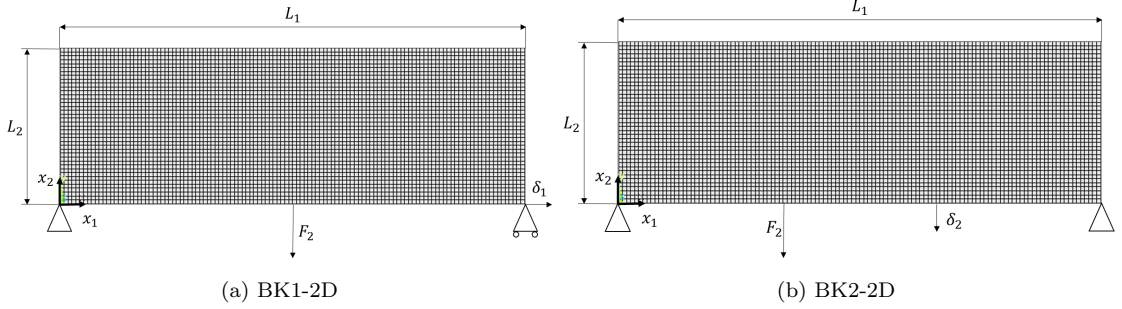


Figure 1: FE model and BCs of benchmark problems (a) BK1-2D and (b)BK2-2D

Three different materials are used for both BK1-2D and BK2-2D. Their properties are listed in Tab. 2 in terms of engineering constants. In particular, M1 is a linear elastic isotropic material, M2 is characterised by a square symmetry behaviour, whilst M3 is an orthotropic material.

**Remark 4.4.** *The material properties used in this work are expressed either in the form of engineering constants or in the form of the Cartesian components of the elasticity tensor in the material frame. In each case, the standard Voigt's notation is used [30]. The passage from tensor notation to Voigt's one can be easily expressed by the following two-way relationship among indices:*

$$\{11, 22, 33, 32, 31, 21\} \Leftrightarrow \{1, 2, 3, 4, 5, 6\}. \quad (38)$$

Material ID	Symmetry type	$E_1$ [MPa]	$E_2$ [MPa]	$G_{12}$ [MPa]	$\nu_{12}$
M01	Isotropy	1.0	1.0	0.3846	0.3
M02	Square symmetry	1.0	1.0	0.0507	0.27
M03	Orthotropy	1.0	0.0725	0.0507	0.27

Table 2: Elastic properties of the materials used for BK1-2D and BK2-2D

#### 4.1.1. BK1-2D: sensitivity of the optimised topology to the applied displacement and to the elastic symmetry group

A campaign of numerical analyses has been conducted on BK1-2D, with the aim of studying the influence of both the applied displacement and the elastic symmetry group on the optimised topology. These sensitivity analyses are carried out only for problem (37) by considering a volume fraction  $\gamma = 0.4$  and the three materials listed in Tab. 2. As discussed in the above subsection, the applied displacement  $\delta_1$  takes values in the interval  $[-40, 40]$  mm with a step of 10 mm.

The minimum dimension, which can be fabricated through the considered manufacturing process appearing in Eq. (35), has been set as  $d_{MP} = 2.5$  mm. As discussed in [16],

this requirement can be satisfied by choosing an appropriate number of CPs and blending functions degree. Therefore, these parameters have been set as  $n_{\text{CP}} = 100 \times 36$  and  $p_j = 2$  ( $j = 1, 2$ ), respectively, according to the methodology described in [16]. Moreover, to analyse the influence of the geometric entity on the optimised topology, both B-spline and NURBS surfaces have been used to solve the CNLPP of Eq. (37).

An initial guess characterised by a uniform pseudo-density field  $\rho(\zeta_1, \zeta_2) = \gamma$  has been considered for each analysis. The reference value of the generalised compliance  $\mathcal{C}_{\text{ref}}$  of the starting guess is reported in Tab. 3 for each combination of material and applied displacement.

Material ID	$\delta_1$ [mm] =								
	-40	-30	-20	-10	0	10	20	30	40
M01	137.7	147.9	157.7	167.0	175.8	184.8	192.1	199.5	206.5
M02	482.5	490.4	497.9	505.2	512.1	518.7	525.0	531.0	536.7
M03	1177.1	1189.4	1201.4	1213.2	1224.7	1235.9	1246.9	1257.6	1268.1

Table 3: BK1-2D: reference value of the generalised compliance  $\mathcal{C}_{\text{ref}}$  [Nmm] used in problem (37) for each combination of material and BCs

The trend of the generalised compliance vs. the applied displacement is illustrated in Figs. 2 - 7. In each figure, the optimised topology and the number of iterations to achieve convergence ( $N_{\text{iter}}$ ), for each value of the applied displacement, are also illustrated. The trend of the generalised compliance vs. the applied displacement has been plotted for both B-spline and NURBS solutions for each material listed in Tab. 2: Figs. 2 and 3 refer to material M01, Figs. 4 and 5 refer to material M02, and Figs. 6 and 7 refer to material M03.

The following remarks can be inferred from the analysis of these results.

1. For each material considered in this study, optimised topologies obtained using NURBS surfaces are characterised by values of the objective function lower than or equal to those resulting from B-spline surfaces. Furthermore, from the analysis of 2 - 7, one can notice that NURBS topologies have a boundary smoother than the one of B-spline solutions. This last aspect is related to the ability of NURBS entities to better approximate quadric hyper-surfaces as widely known in the CAD community.
2. One can notice that the use of NURBS entities as topological descriptors allows better exploring the design space when compared to the case of B-spline entities. The optimised topologies obtained through NURBS surfaces are significantly different from those obtained through B-spline entities for some combinations of material and applied displacement. These differences are particularly pronounced for the optimal solutions obtained in: a) the isotropic case (M01) for  $\delta_1 = 10$  mm, 20 mm (see Figs. 2 and 3); b) the square symmetry case (M02) for  $\delta_1 = -30$  mm, -20 mm, 10 mm, 20 mm (see Figs. 4 and 5); c) the orthotropic case (M03) for  $\delta_1 = 0$  mm, 10 mm (see Figs. 6 and 7).
3. The optimised topologies obtained in the isotropic case are characterised by the lowest value of the generalised compliance (for each value of the applied displacement  $\delta_1$ ). This is due to the nature of the stress state within the structure (i.e., a multi-axial stress field) which is better withstood by an isotropic material rather than by a material characterised by a square symmetry or by an orthotropic behaviour.
4. The optimised topologies obtained in the orthotropic case do not fill the whole design domain, regardless of the value of the applied displacement  $\delta_1$ . Conversely, the material is essentially distributed along the  $x_1$  axis on the bottom part of the domain

(i.e., where forces and displacement are applied). This is an expected result because the main axis of orthotropy is aligned with  $x_1$  axis (see Tab. 2).

5. It is noteworthy that, depending on the value of the applied displacement  $\delta_1$ , the generalised compliance can take negative values, meaning, thus, that this functional is not positive definite.
6. For each solution, the minimum length scale requirement is systematically fulfilled thanks to the local support property of the NURBS entities, which establishes an implicit filter according to Eq. (9). In particular, the lowest thickness (which is equal to 2.55 mm) occurs in the square symmetry case for  $\delta_1 = -30$  mm for the NURBS solution shown in Fig. 5.

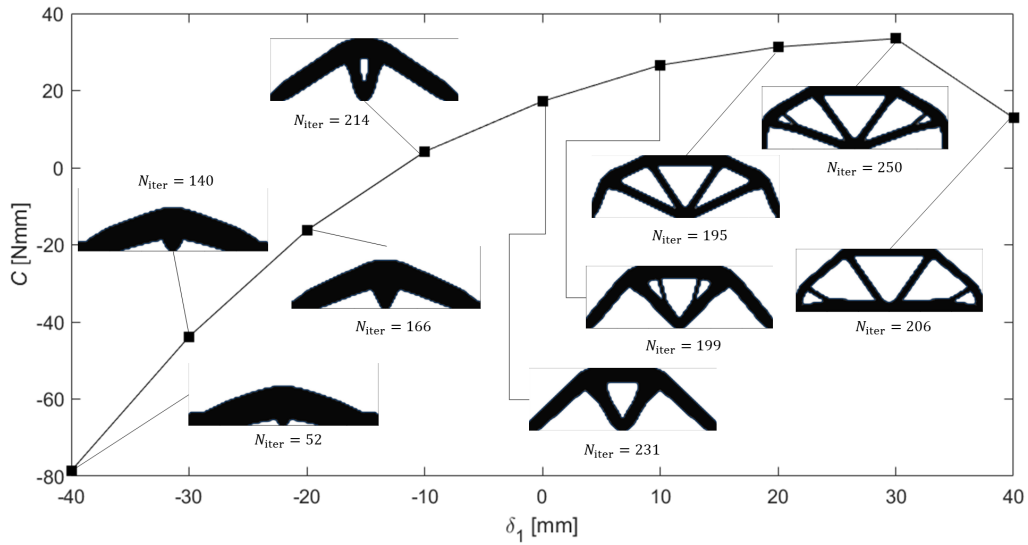


Figure 2: BK1-2D: generalised compliance vs. applied displacement for material M01 - B-spline solutions

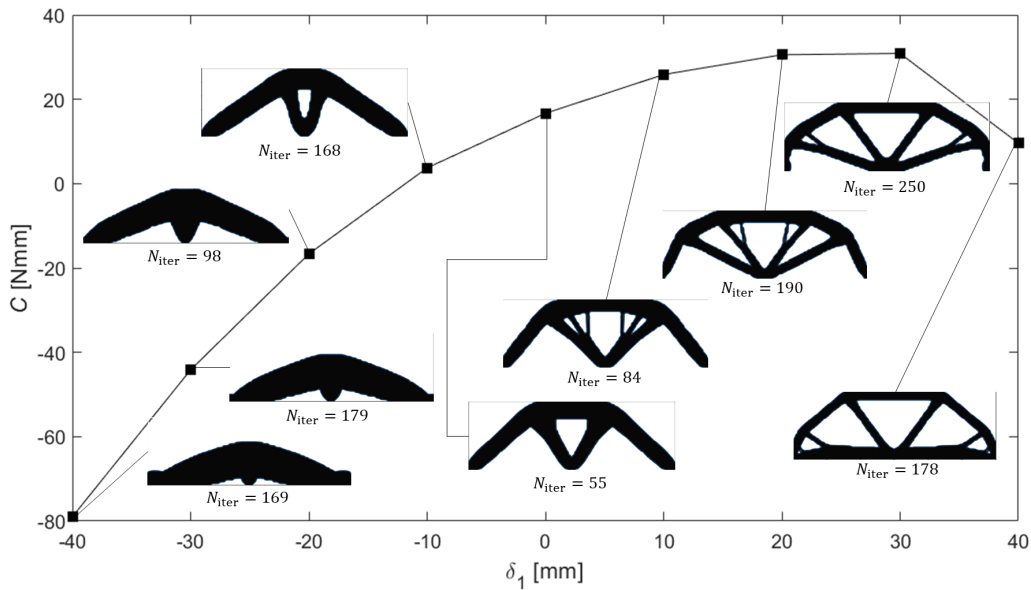


Figure 3: BK1-2D: generalised compliance vs. applied displacement for material M01 - NURBS solutions

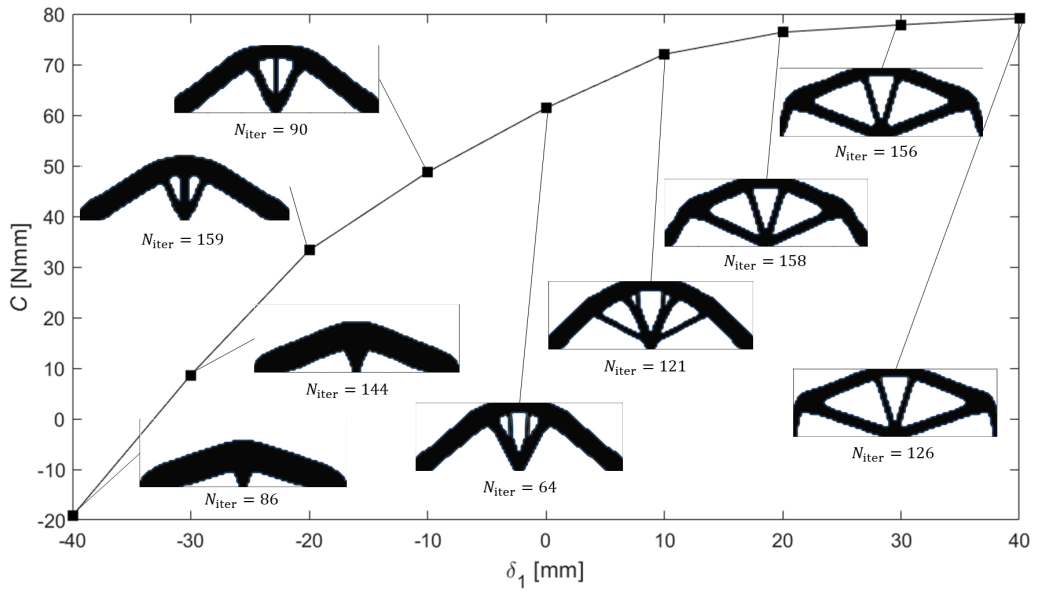


Figure 4: BK1-2D: generalised compliance vs. applied displacement for material M02 - B-spline solutions

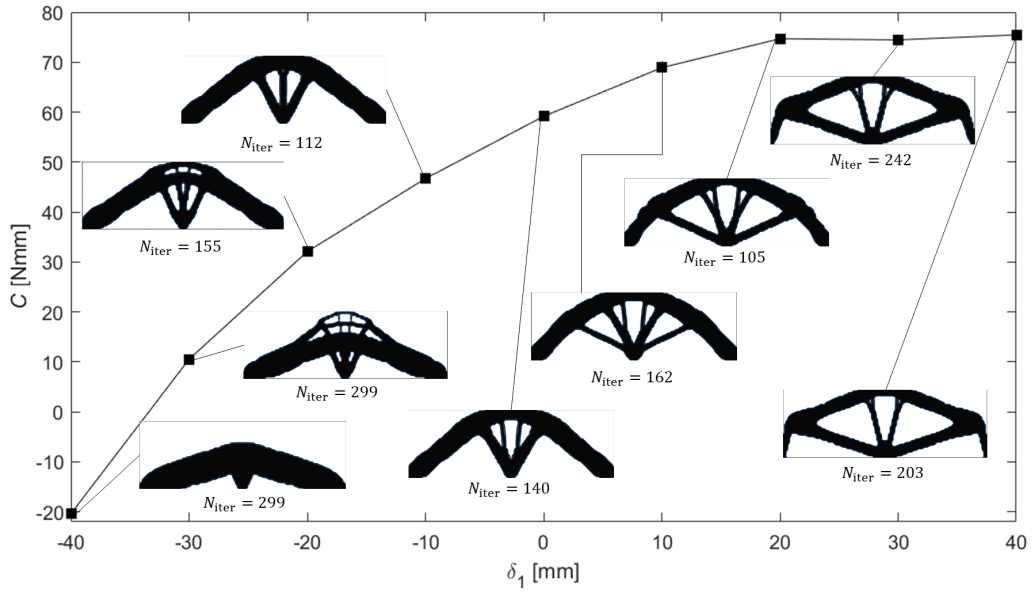


Figure 5: BK1-2D: generalised compliance vs. applied displacement for material M02 - NURBS solutions

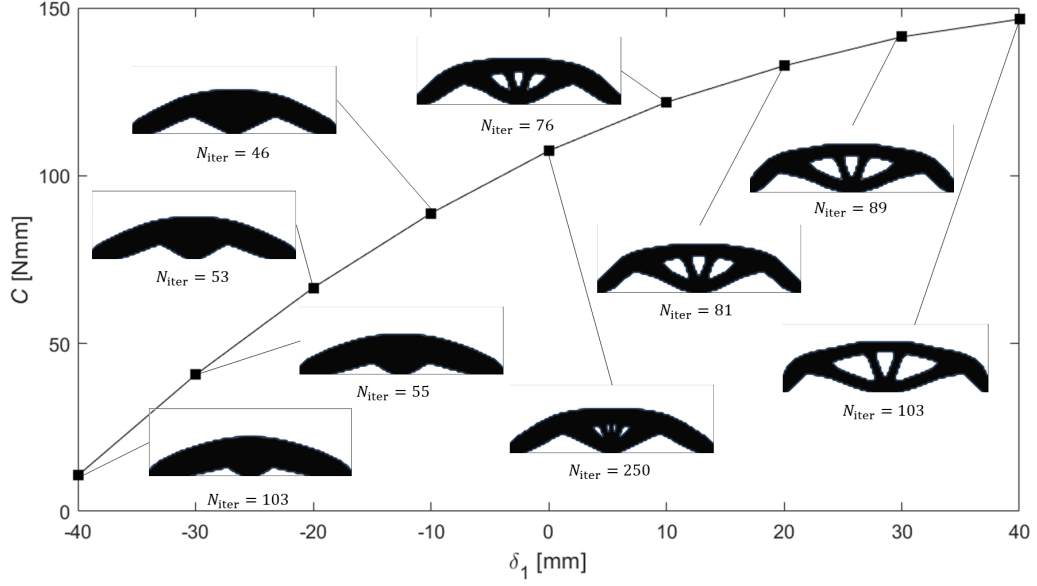


Figure 6: BK1-2D: generalised compliance vs. applied displacement for material M03 - B-spline solutions

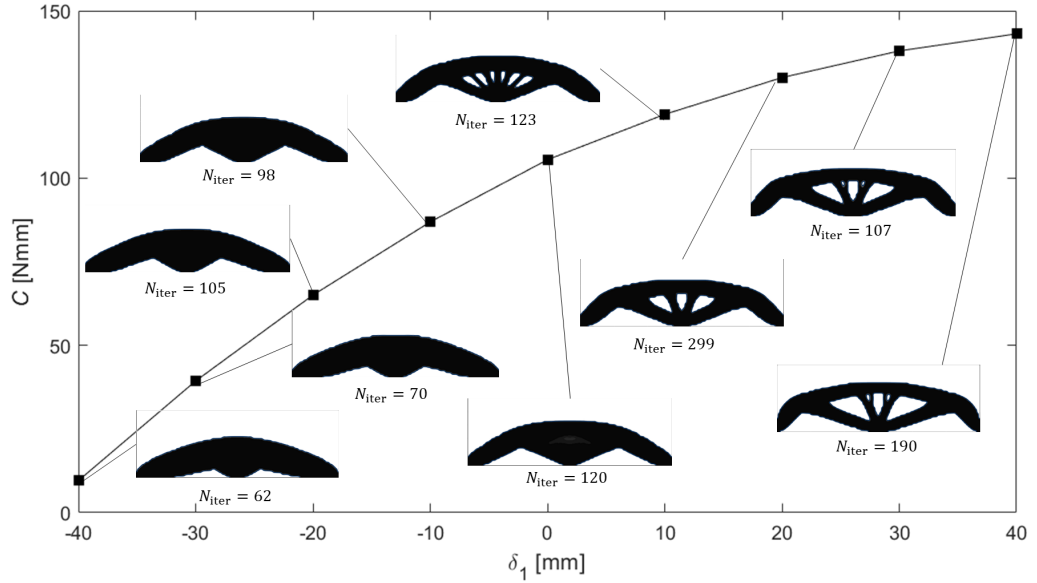


Figure 7: BK1-2D: generalised compliance vs. applied displacement for material M03 - NURBS solutions

#### 4.1.2. BK2-2D: sensitivity of the optimised topology to the volume fraction and to the elastic symmetry group

The goal of the numerical analyses performed on BK2-2D is to study the influence of both the volume fraction and the elastic symmetry group on the optimised topology. Moreover, these analyses are carried out for both problem formulations of Eqs. (36) and (37). For each CNLPP, the volume fraction  $\gamma$  takes value in the interval  $[0.15, 0.45]$  with a step of 0.1 and the TO calculation is performed for each of the three materials listed in Tab. 2.

To analyse the influence of the geometric entity on the optimised topology, the CNLPPs of Eqs. (36) and (37) have been solved by using both B-spline and NURBS surfaces. The integer parameters involved in their definition have been set as follows:  $n_{CP} = 100 \times 36$

and  $p_j = 2$  ( $j = 1, 2$ ). As explained in the above subsection, according to the methodology discussed in [16], this choice ensures a minimum member size greater than or equal to  $d_{MP} = 2.5$  mm.

An initial guess characterised by a uniform pseudo-density field  $\rho(\zeta_1, \zeta_2) = \gamma$  has been considered for each analysis. The reference values of both the WAFD and the generalised compliance of the starting guess are reported in Tabs. 4 and 5 for each combination of volume fraction value and material considered in the analysis.

Material ID	$\gamma =$			
	0.15	0.25	0.35	0.45
M01	2724.3	540.8	190.4	88.3
M02	7761.2	1540.6	541.9	250.2
M03	22176.1	4401.9	1548.2	714.4

Table 4: BK2-2D: reference value of the WAFD  $\mathcal{W}_{ref}$  [Nmm] used in problem (36) for each combination of material and volume fraction  $\gamma$

Material ID	$\gamma =$			
	0.15	0.25	0.35	0.45
M01	2732.2	548.6	197.8	95.1
M02	7769.2	1548.5	549.7	257.8
M03	22182.8	4408.6	1555.0	721.1

Table 5: BK2-2D: reference value of the generalised compliance  $\mathcal{C}_{ref}$  [Nmm] used in problem (37) for each combination of material and volume fraction  $\gamma$

The trend of the objective function vs. the volume fraction for both CNLPPs of Eqs. (36) and (37) is illustrated in Figs. 8 - 13. In each figure, the optimised topology and the number of iterations to achieve convergence ( $N_{iter}$ ), for each value of the volume fraction, are also illustrated. The trend of the objective function vs. the volume fraction has been plotted for both B-spline and NURBS solutions for each material listed in Tab. 2: Figs. 8 and 9 refer to material M01, Figs. 10 and 11 refer to material M02, and Figs. 12 and 13 refer to material M03.

From the analysis of these results, one can infer the following remarks.

1. As in the case of BK1-2D, for each material considered in this study, optimised topologies obtained using NURBS surfaces are characterised by values of the objective function lower than or equal to those resulting from B-spline surfaces. Furthermore, as expected, NURBS topologies have a boundary smoother than the one of B-spline solutions. However, the greater the volume fraction the lower the difference between the values of the objective function obtained through B-spline and NURBS surfaces, respectively.
2. As illustrated in Figs. 8 and 9 for B-spline and NURBS solutions, respectively, in the isotropic case (material M01) the optimised topologies resulting from the two problem formulations are quite different. In particular, the higher the volume fraction the more important the difference, especially in the right-bottom part of the domain, i.e, for the region located on the right of the nodes where the vertical displacement  $\delta_2$  is applied. Moreover, regarding the optimal solution of problem (37) obtained for  $\gamma = 0.35$ , there is a fundamental difference between B-spline and NURBS surfaces: the topology obtained when a NURBS entity is used as a topological descriptor is characterised by a vertical branch, a feature which does not appear in the B-spline

counterpart. Although this difference, both optimised topologies constitute “equivalent” local minima (the value of the generalised compliance is almost the same), meaning that the CNLPP of Eq. (37) is highly non-convex.

3. Remarkably, the optimised topologies resulting from the two problem formulations of Eqs. (36) and (37) are the same for materials M02 (square symmetry behaviour, see Figs. 10 and 11, for B-spline and NURBS entities, respectively) and M03 (orthotropic behaviour, see Figs. 12 and 13, for B-spline and NURBS entities, respectively). This is an unexpected result: it seems that the elastic symmetry of the material acts as a filter against the sensitivity of the topology to the objective function, regardless of the value of the volume fraction. Probably, in the considered design domain and under the imposed BCs, the merit functions  $\mathcal{W}_{\text{ref}}$  and  $\mathcal{C}_{\text{ref}}$  are characterised by a similar trend and share the same local minima. A deeper investigation on the mathematical nature of these functions and of problems (36) and (37) is needed to clarify this point, but this task is outside the scopes of the present study.
4. Thanks to the geometrical properties of the NURBS blending functions, the requirement on the minimum length scale is always satisfied. In particular, it is noteworthy that the lowest thickness (which is equal to 2.6 mm) occurs in the isotropic case for  $\gamma = 0.15$  and for the NURBS solution of problem (37) (as shown in Fig. 9b).

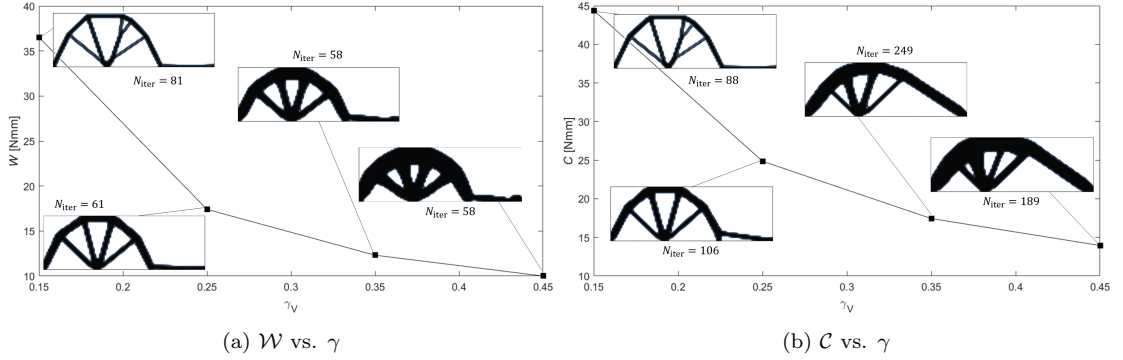


Figure 8: BK2-2D: objective function vs. volume fraction for a) problem (36) and b) problem (37); material M01 - B-spline solutions.

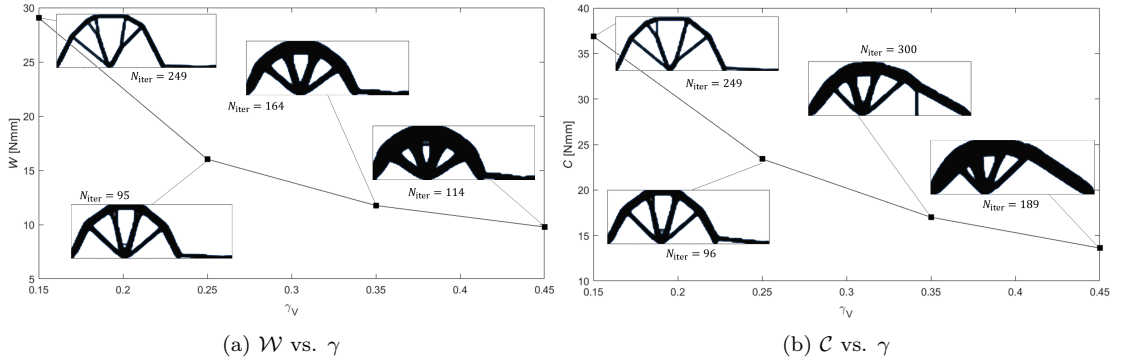


Figure 9: BK2-2D: objective function vs. volume fraction for a) problem (36) and b) problem (37); material M01 - NURBS solutions.

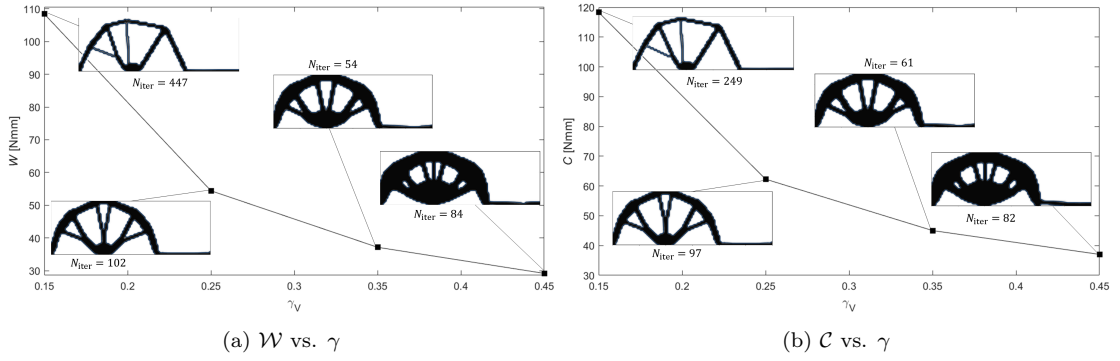


Figure 10: BK2-2D: objective function vs. volume fraction for a) problem (36) and b) problem (37); material M02 - B-spline solutions.

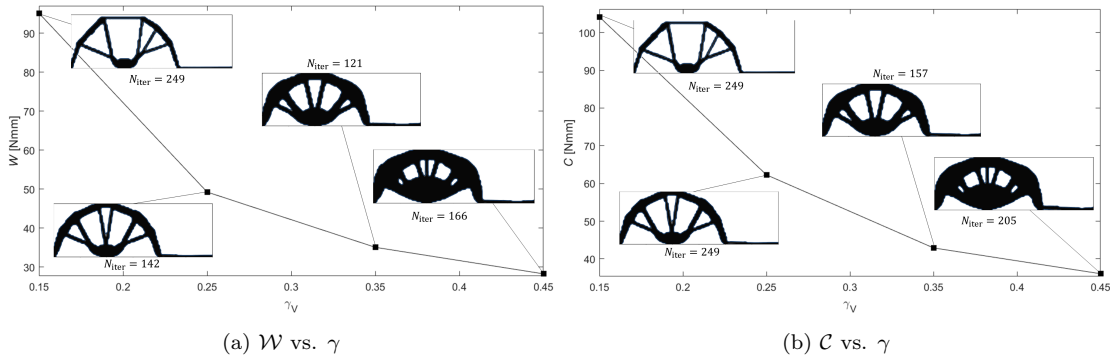


Figure 11: BK2-2D: objective function vs. volume fraction for a) problem (36) and b) problem (37); material M02 - NURBS solutions.

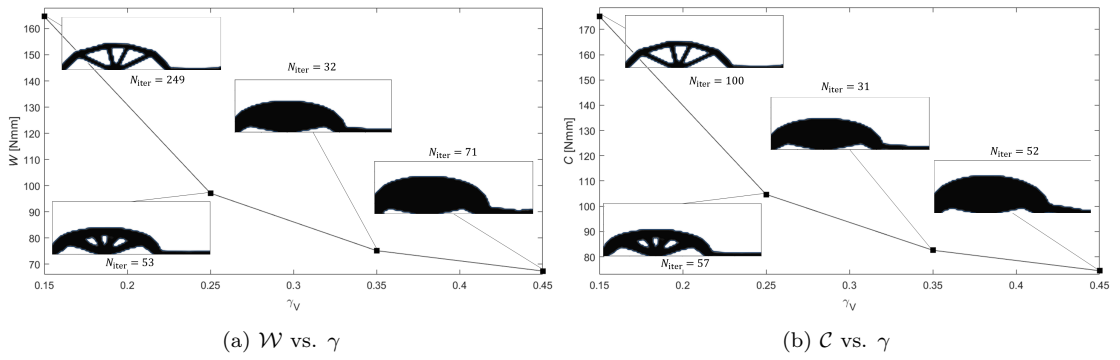


Figure 12: BK2-2D: objective function vs. volume fraction for a) problem (36) and b) problem (37); material M03 - B-spline solutions.

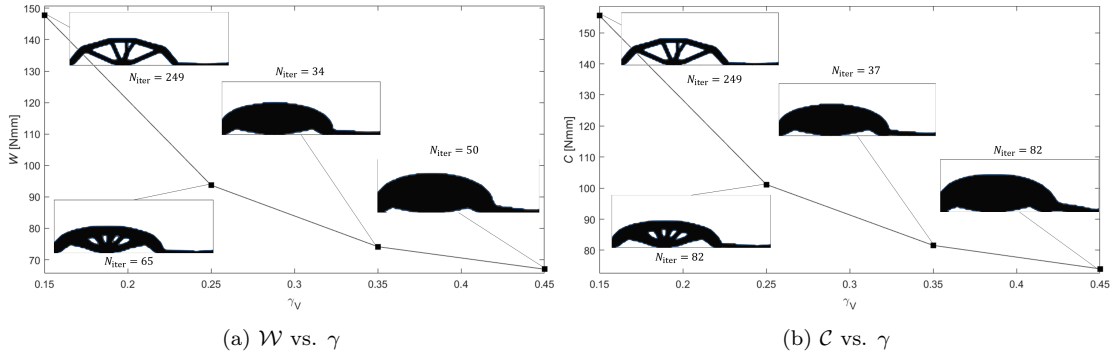


Figure 13: BK2-2D: objective function vs. volume fraction for a) problem (36) and b) problem (37); material M03 - NURBS solutions.

#### 4.2. 3D benchmark problem

The geometry and the FE model of the 3D benchmark problem (BK3D) are shown in Fig. 14. The design domain is a cube with size  $L_j = 200$  mm ( $j = 1, 2, 3$ ). The FE model is composed of  $N_e = 30 \times 30 \times 30$  SOLID185 elements (i.e., solid elements with eight nodes and three DOFs per node, full integration scheme). Mixed BCs are applied as follows:

- Nodes located at  $(x_1, x_2, x_3) = (iL_1, jL_2, 0)$  ( $i, j = 0, 1$ ) are clamped (i.e.,  $u_k = 0$ ,  $k = 1, 2, 3$ );
- A force  $F_3 = 1$  N is applied at the node located at  $(x_1, x_2, x_3) = (\frac{L_1}{2}, \frac{L_2}{2}, L_3)$ ;
- Displacements  $u_1 = \delta_1$  and  $u_1 = -\delta_1$  are applied at nodes located at  $(x_1, x_2, x_3) = (L_1, 0, L_3)$  and  $(x_1, x_2, x_3) = (0, L_2, L_3)$ , respectively, with  $\delta_1 = 1$  mm;
- Displacements  $u_2 = \delta_2$  and  $u_2 = -\delta_2$  are applied at nodes located at  $(x_1, x_2, x_3) = (L_1, L_2, L_3)$  and  $(x_1, x_2, x_3) = (0, 0, L_3)$ , respectively, with  $\delta_2 = 1$  mm.

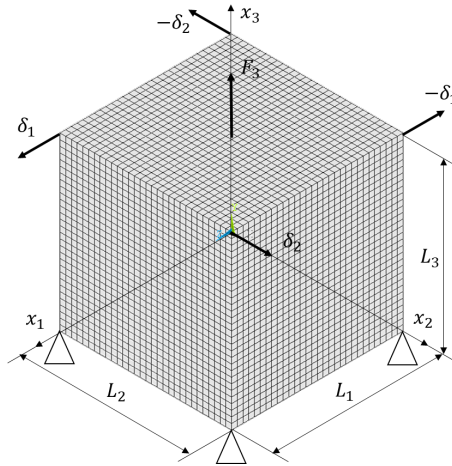


Figure 14: FE model and BCs of benchmark problem BK3D

The influence of the elastic symmetry type on the optimised topology is investigated by considering only the CNLPP formulation of (37), for the sake of brevity. To this end, 11 different materials characterised by various elastic symmetries are considered for BK3D: their elastic properties (and the related symmetry group) are reported in Tab. 6 in terms of the components of the elasticity tensor (Voigt's notation).

Material ID	Symmetry type	$C_0$ [MPa]					
M01	Isotropy	1.0	0.4286	0.4286	0	0	0
		0.4286	1.0	0.4286	0	0	0
		0.4286	0.4286	1.0	0	0	0
		0	0	0	0.2857	0	0
		0	0	0	0	0.2857	0
		0	0	0	0	0	0.2857
M02	Cubic syngony	1.0	0.8400	0.8400	0	0	0
		0.8400	1.0	0.8400	0	0	0
		0.8400	0.8400	1.0	0	0	0
		0	0	0	0.6000	0	0
		0	0	0	0	0.6000	0
		0	0	0	0	0	0.6000
M03	Cubic syngony	1.0	0.5363	0.5363	0	0	0
		0.5363	1.0	0.5363	0	0	0
		0.5363	0.5363	1.0	0	0	0
		0	0	0	0.1165	0	0
		0	0	0	0	0.1165	0
		0	0	0	0	0	0.1165
M04	Monoclinic	0.5455	0.2000	0.2400	0	0	0.1091
		0.2000	0.6327	0.2545	0	0	0.0364
		0.2400	0.2545	1.0	0	0	0.0345
		0	0	0	0.2527	0.0527	0
		0	0	0	0.0527	0.1964	0
		0.1091	0.0364	0.0345	0	0	0.2727
M05	Orthotropy	0.9610	0.2332	0.4445	0	0	0
		0.2332	0.8602	0.2865	0	0	0
		0.4445	0.2865	1.0	0	0	0
		0	0	0	0.2396	0	0
		0	0	0	0	0.2050	0
		0	0	0	0	0	0.3497
M06	Hexagonal syngony	1.0	0.5843	0.3449	0	0	0
		0.5843	1.0	0.3449	0	0	0
		0.3449	0.3449	0.6792	0	0	0
		0	0	0	0.2003	0	0
		0	0	0	0	0.2003	0
		0	0	0	0	0	0.2078
M07	Hexagonal syngony	0.4875	0.1371	0.3047	0	0	0
		0.1371	0.4875	0.3172	0	0	0
		0.3047	0.3172	1.0	0	0	0
		0	0	0	0.0346	0	0
		0	0	0	0	0.0346	0
		0	0	0	0	0	0.1745
M08	Hexagonal syngony	0.9257	0.4662	0.3784	0	0	0
		0.4662	0.9257	0.3784	0	0	0
		0.3784	0.3784	1.0	0	0	0
		0	0	0	0.2027	0	0
		0	0	0	0	0.2027	0
		0	0	0	0	0	0.2297
M09	Hexagonal syngony	1.0	0.5907	0.4643	0	0	0
		0.5907	1.0	0.4643	0	0	0
		0.4643	0.4643	0.6420	0	0	0
		0	0	0	0.3653	0	0
		0	0	0	0	0.3653	0
		0	0	0	0	0	0.2047
M10	Trigonal syngony	0.8074	0.0660	0.1340	0.1600	0	0
		0.0660	0.8074	0.1340	-0.1600	0	0
		0.1340	0.1340	1.0	0	0	0
		0.1600	-0.1600	0	0.5414	0	0
		0	0	0	0	0.5414	0.1600
		0	0	0	0	0.1600	0.3707
M11	Transverse isotropy	0.0446	0.0109	0.0129	0	0	0
		0.0109	0.0446	0.0129	0	0	0
		0.0129	0.0129	1.0	0	0	0
		0	0	0	0.0743	0	0
		0	0	0	0	0.0743	0
		0	0	0	0	0	0.0168

Table 6: Elasticity tensor and symmetry type of the materials used for BK3D

**Remark 4.5.** *It is noteworthy that, with the exception of materials M01 (isotropic case), M06 and M09 (hexagonal syngony case), the “strong” axis of the material is aligned with  $x_3$  axis.*

**Remark 4.6.** *The number of independent elastic properties depends, of course, on the elastic symmetry type to which the material belongs to. In the case of the materials listed in Tab. 6 such number is equal to: 2 for M01, 3 for M02 and M03, 13 for M04, 9 for M05, 5 for M06-M09, 6 for M10, 5 for M11.*

The CNLPP formulation of (37) has been enhanced by introducing a requirement on the minimum member size: the minimum dimension of the optimised topology should be greater than or equal to  $d_{\text{MP}} = 5.0$  mm. To satisfy the minimum length scale requirement without introducing an explicit constraint in the problem formulation, the approach discussed in [16] is used also in this case. Accordingly, a B-spline entity with  $p_j = 2$  ( $j = 1, 2, 3$ ) and  $n_{\text{CP}} = 28 \times 28 \times 28$  CPs is used for these analyses.

Following the same approach used for 2D problems, an initial guess characterised by a uniform pseudo-density field  $\rho(\zeta_1, \zeta_2) = \gamma$  has been considered for each analysis. The reference value of the generalised compliance  $\mathcal{C}_{\text{ref}}$  of the starting guess is reported in Tab. 3 for each material used in the optimisation process.

A synthesis of the results, in terms of the value of the generalised compliance  $\mathcal{C}$  characterising the optimised topology, for each material considered for BK3D, is shown in Fig. 15. The optimised topologies obtained for each material of Tab. 6 are illustrated in Fig. 16, wherein the number of iterations to achieve convergence is also reported. The following remarks can be drawn from the analysis of these results.

1. A negative value of the generalised compliance is found only when using materials M01 (isotropy), M02 (cubic syngony), M09 (hexagonal syngony) and M10 (trigonal syngony).
2. The optimised topologies for materials belonging to the same elastic symmetry group (like M02 and M03, or M06-M09) show some differences. In particular, among materials characterised by cubic syngony (M02 and M03), material M02 is characterised by the lowest value of  $\mathcal{C}$ , whereas among materials characterised by a hexagonal symmetry (M06-M09), material M09 show the best behaviour in terms of structural stiffness. Among materials M02 and M09, the latter show better performances in terms of generalised compliance. This is an unexpected result, especially for materials belonging to the hexagonal symmetry class, because the main axes of symmetry for material M09 are oriented along  $x_1$  and  $x_2$  directions.
3. All the optimised topologies are characterised by a (geometric) axial symmetry of order four around  $x_3$  axis (i.e., the geometry does not change when applying a rotation of 90 deg around this axis), except the one obtained for material M10 (trigonal symmetry), which is completely asymmetric. Remarkably, the optimised topology obtained for material M10 is also the one showing the lowest value of  $\mathcal{C}$ , whilst the one obtained for material M07 (hexagonal syngony) show the highest value of  $\mathcal{C}$ . This is an unexpected result that could be due to the strong non-convex nature of the CNLPP of Eq. (37) when using a material with trigonal syngony behaviour. A deeper investigation on the mathematical nature of the functional  $\mathcal{C}$  (which is outside the scopes of the present work) could provide a deeper understanding of this behaviour.
4. For each solution, the minimum length scale requirement is systematically fulfilled: the lowest thickness (which is equal to 6.7 mm) occurs in the transversely isotropic case (M11) as illustrated in Fig. 16.

M01	M02	M03	M04	M05	M06	M07	M08	M09	M10	M11
31.8	25.9	56.3	36.4	36.3	43.7	105.2	37.9	34.9	22.0	76.9

Table 7: BK3D: reference value of the generalised compliance  $C_{\text{ref}}$  [Nmm] used in problem (37) for each material listed in Tab. 6

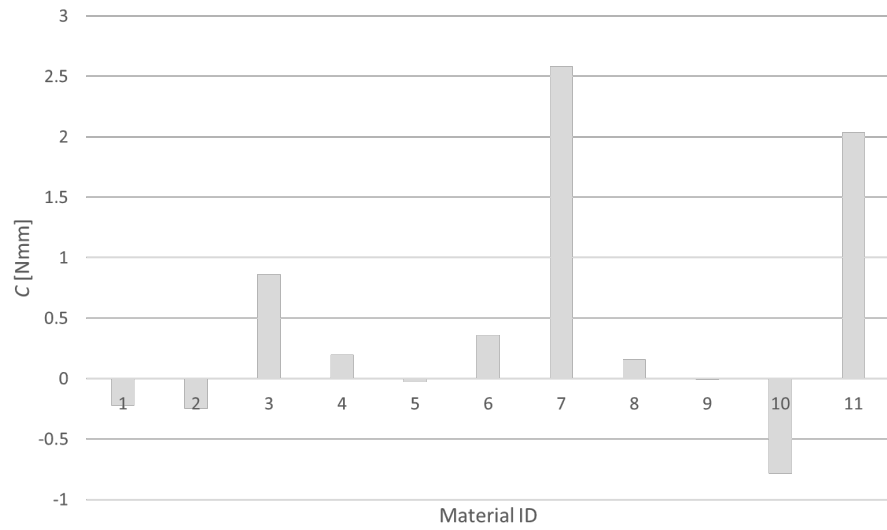
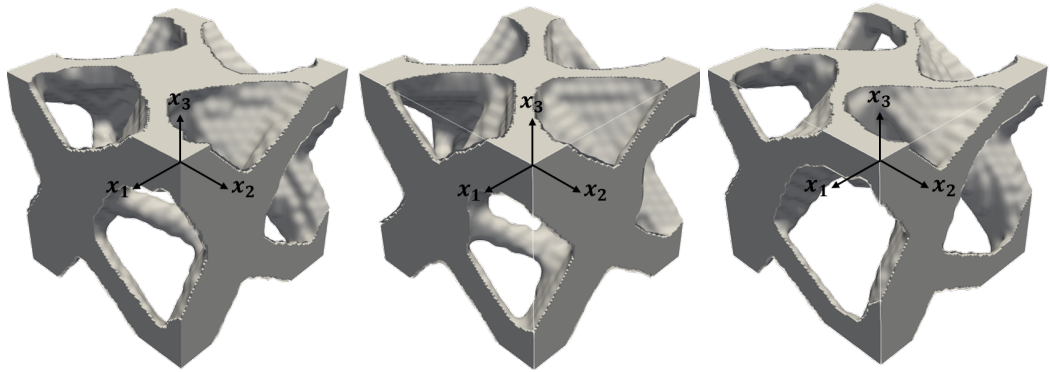
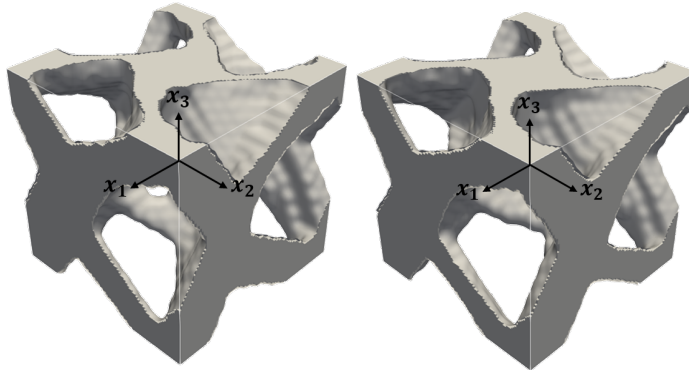


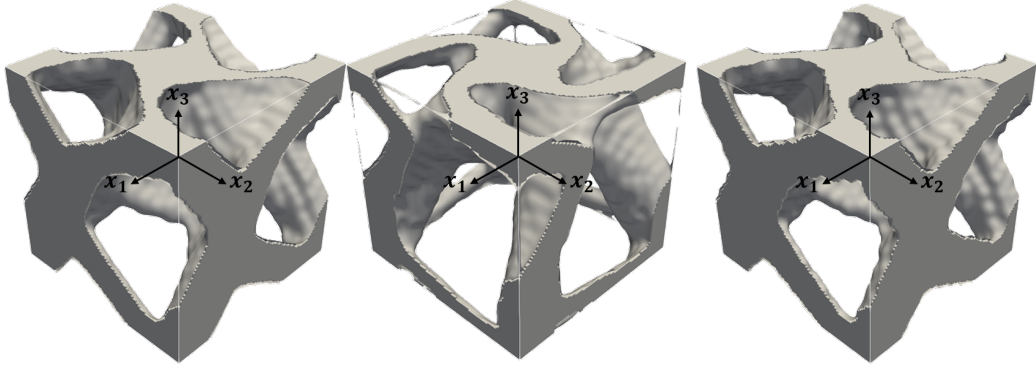
Figure 15: BK3D: generalised compliance vs. material type for the optimised topologies solution of problem (37)



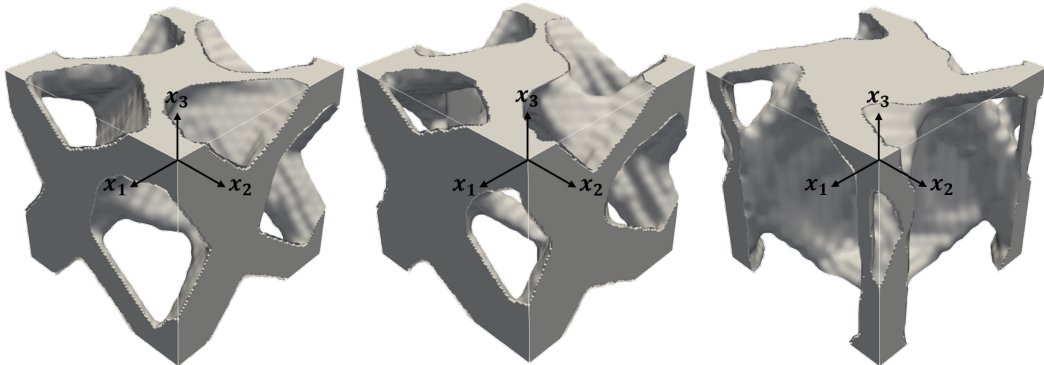
(a)  $C = -0.23$  Nmm,  $N_{\text{iter}} = 299$ , M01 (b)  $C = -0.25$  Nmm,  $N_{\text{iter}} = 299$ , M02 (c)  $C = 0.86$  Nmm,  $N_{\text{iter}} = 299$ , M03



(d)  $C = 0.20$  Nmm,  $N_{\text{iter}} = 299$ , M04 (e)  $C = -0.03$  Nmm,  $N_{\text{iter}} = 299$ , M05



(f)  $C = 0.36$  Nmm,  $N_{\text{iter}} = 162$ , M06 (g)  $C = 2.58$  Nmm,  $N_{\text{iter}} = 299$ , M07 (h)  $C = 0.16$  Nmm,  $N_{\text{iter}} = 299$ , M08



(i)  $C = -0.01$  Nmm,  $N_{\text{iter}} = 299$ , M09 (j)  $C = -0.79$  Nmm,  $N_{\text{iter}} = 299$ , M10 (k)  $C = 2.03$  Nmm,  $N_{\text{iter}} = 299$ , M11

Figure 16: BK3D: optimised topologies solution of problem (37) by considering different materials.

## 5. Conclusions

In this work, three theoretical aspects of TO problems dealing with structural stiffness maximisation of anisotropic continua under mixed non-zero ND BCs have been discussed.

Firstly, it has been shown that the most natural measure of the structural stiffness is the so-called generalised compliance, i.e., a functional related to the TPE of the continuum, rather than the WAFD.

Secondly, it has been proved that the WAFD is not a self-adjoint functional under mixed non-zero ND BCs, whilst the generalised compliance is always a self-adjoint functional (a proof simpler than the one available in the literature has been provided in this study).

Thirdly, a large campaign of analyses has been conducted to study the influence of the anisotropy, of the applied BCs and of the design requirement on the volume fraction on the optimised topology. All the calculations have been carried out in the framework of a topology optimisation algorithm making use of NURBS hyper-surfaces to represent the pseudo-density field of the SIMP method.

Some features of the proposed methodology need to be highlighted.

1. Depending on the elastic symmetry type of the continuum and on the value of the volume fraction, the optimal solutions of the two problem formulations (i.e. the one based on the generalised compliance and the one based on the WAFD) can coincide.
2. Depending on the value of the applied displacements and on the elastic symmetry type of the material, the generalised compliance can take negative values, confirming thus the non-positiveness of this functional.
3. Depending on the elastic symmetry type, the optimised topologies characterised by the best performances, in terms of structural stiffness, could be totally asymmetric.
4. For a given elastic symmetry type, a given volume fraction and given applied displacements, different topologies could show the same structural response either in terms of generalised compliance or in terms of work of WAFD. This is due to the strong non-convexity of the optimisation problem and to the existence of equivalent local minima.
5. The manufacturing constraint related to the minimum-length scale is correctly taken into account, without the need of introducing an explicit optimisation constraint. Indeed, such technological constraint is handled by controlling the value of the blending functions degrees and the number of control points of the NURBS entity.
6. Some advantages of the NURBS formalism can be clearly identified: (a) since the topological descriptor consists in a high-level geometric parametrisation of the pseudo-density field in the form of a NURBS entity, the optimised topology does not depend upon the quality of the mesh of the finite element model; (b) unlike the classical SIMP approach, there is no need to define a further filter zone, since the NURBS local support property establishes an implicit relationship among contiguous mesh elements; (c) when compared to the classical SIMP approach, the number of design variables is reduced; (d) since the topology is described through a NURBS entity, the boundary of the topology is available at each iteration of the optimisation process, thus, the integration of constraints of geometric nature (e.g., on the local curvature of the boundary, on the local direction of the tangent vector, maximum member size, etc.) in the problem formulation and the CAD reconstruction phase of the boundary of the optimised topology become easy tasks; (e) of course, the optimised topology depends upon the NURBS integer parameters, i.e., number of

control points and degrees of Bernstein's polynomials, which have a direct impact on the size of the local support of the blending functions.

As far as the prospects of this work are concerned, several challenges still need to be faced. Firstly, the formulation proposed here should be extended to the problem of the concurrent optimisation of the local nature of the material (i.e., the optimisation of the type of elastic symmetry and of the direction of such symmetry) and of the topology of the structure under mixed non-zero ND BCs.

Furthermore, the effect of the elastic symmetry type on the optimised topology and the (possible) strong coupling among anisotropy and topology should be properly investigated by using a representation of anisotropy based on (tensor) invariants related to the elastic symmetries of the materials. To the best of the author's knowledge, unfortunately, such a representation is available only in the 2D case, whilst is still missing in the most general 3D case. Indeed, a closed form representation of the elasticity tensor through invariants related to all the possible elastic symmetries of a material is still an open problem in the scientific community.

Research is ongoing on the above aspects.

## Data availability

The raw/processed data required to reproduce these findings cannot be shared at this time as the data also forms part of an ongoing study.

## A. Gradient of the work of applied forces and displacements under mixed boundary conditions

The proof of Prop. 3.1, provided here below, makes use of the adjoint method [31].

*Proof.* Under the application of non-zero mixed BCs, and by considering Eq. (15), the WAFD of Eq. (19) can be written as follows:

$$\mathcal{W} = \mathbf{f}^T \mathbf{u} + \mathbf{u}_{\text{BC}}^T \mathbf{r} + \boldsymbol{\eta}^T (\mathbf{K} \mathbf{u} + \mathbf{K}_{\text{BC}} \mathbf{u}_{\text{BC}} - \mathbf{f}) + \boldsymbol{\lambda}^T (\mathbf{K}_{\text{BC}}^T \mathbf{u} + \tilde{\mathbf{K}} \mathbf{u}_{\text{BC}} - \mathbf{r}), \quad (\text{A.1})$$

where  $\boldsymbol{\eta} \in \mathbb{R}^{N_{\text{DOF}}}$  and  $\boldsymbol{\lambda} \in \mathbb{R}^{N_{\text{BC}}}$  are two arbitrary vectors. Under the hypothesis that vectors  $\mathbf{f}$  and  $\mathbf{u}_{\text{BC}}$  do not depend on the TV, i.e.,

$$\frac{\partial \mathbf{f}}{\partial \xi_{i\tau}} = \mathbf{0}, \quad \frac{\partial \mathbf{u}_{\text{BC}}}{\partial \xi_{i\tau}} = \mathbf{0}, \quad (\text{A.2})$$

the derivative of Eq. (A.1) reads:

$$\begin{aligned} \frac{\partial \mathcal{W}}{\partial \xi_{i\tau}} = & \mathbf{f}^T \frac{\partial \mathbf{u}}{\partial \xi_{i\tau}} + \mathbf{u}_{\text{BC}}^T \frac{\partial \mathbf{r}}{\partial \xi_{i\tau}} + \\ & + \boldsymbol{\eta}^T \left( \frac{\partial \mathbf{K}}{\partial \xi_{i\tau}} \mathbf{u} + \mathbf{K} \frac{\partial \mathbf{u}}{\partial \xi_{i\tau}} + \frac{\partial \mathbf{K}_{\text{BC}}}{\partial \xi_{i\tau}} \mathbf{u}_{\text{BC}} \right) + \\ & + \boldsymbol{\lambda}^T \left( \frac{\partial \mathbf{K}_{\text{BC}}^T}{\partial \xi_{i\tau}} \mathbf{u} + \mathbf{K}_{\text{BC}}^T \frac{\partial \mathbf{u}}{\partial \xi_{i\tau}} + \frac{\partial \tilde{\mathbf{K}}}{\partial \xi_{i\tau}} \mathbf{u}_{\text{BC}} - \frac{\partial \mathbf{r}}{\partial \xi_{i\tau}} \right). \end{aligned} \quad (\text{A.3})$$

In Eq. (A.3), vectors  $\boldsymbol{\eta}$  and  $\boldsymbol{\lambda}$  can be chosen such that the terms multiplying  $\frac{\partial \mathbf{u}}{\partial \xi_{i\tau}}$  and  $\frac{\partial \mathbf{r}}{\partial \xi_{i\tau}}$  vanish, i.e.

$$\begin{aligned}\boldsymbol{\lambda} &= \mathbf{u}_{\text{BC}}, \\ \mathbf{K}\boldsymbol{\eta} &= -\mathbf{f} - \mathbf{K}_{\text{BC}}\boldsymbol{\lambda} = -\mathbf{f} - \mathbf{K}_{\text{BC}}\mathbf{u}_{\text{BC}} = \mathbf{K}\mathbf{u} - 2\mathbf{f}, \Rightarrow \boldsymbol{\eta} = \mathbf{u} - 2\mathbf{u}_0,\end{aligned}\tag{A.4}$$

where  $\mathbf{u}_0$  is the solution of Eq. (27). By injecting Eq. (A.4) in Eq. (A.3) one obtains:

$$\begin{aligned}\frac{\partial \mathcal{W}}{\partial \xi_{i\tau}} &= \mathbf{u}^{\text{T}} \frac{\partial \mathbf{K}}{\partial \xi_{i\tau}} \mathbf{u} + 2\mathbf{u}^{\text{T}} \frac{\partial \mathbf{K}_{\text{BC}}}{\partial \xi_{i\tau}} \mathbf{u}_{\text{BC}} + \mathbf{u}_{\text{BC}}^{\text{T}} \frac{\partial \tilde{\mathbf{K}}}{\partial \xi_{i\tau}} \mathbf{u}_{\text{BC}} - 2\mathbf{u}_0^{\text{T}} \left( \frac{\partial \mathbf{K}}{\partial \xi_{i\tau}} \mathbf{u} + \frac{\partial \mathbf{K}_{\text{BC}}}{\partial \xi_{i\tau}} \mathbf{u}_{\text{BC}} \right) \\ &= \hat{\mathbf{u}}^{\text{T}} \frac{\partial \hat{\mathbf{K}}}{\partial \xi_{i\tau}} \hat{\mathbf{u}} - 2\mathbf{u}_0^{\text{T}} \left( \frac{\partial \mathbf{K}}{\partial \xi_{i\tau}} \mathbf{u} + \frac{\partial \mathbf{K}_{\text{BC}}}{\partial \xi_{i\tau}} \mathbf{u}_{\text{BC}} \right).\end{aligned}\tag{A.5}$$

By considering the expression of the non-reduced stiffness matrix of the FE model of the RVE of Eq. (17) and by taking advantage from the local support property of Eq. (9), the first term on the right-hand side of Eq. (A.5) can be simplified as:

$$\begin{aligned}\hat{\mathbf{u}}^{\text{T}} \frac{\partial \hat{\mathbf{K}}}{\partial \xi_{i\tau}} \hat{\mathbf{u}} &= \sum_{e \in \mathcal{S}_\tau} \frac{\alpha}{\rho_e} \frac{\partial \rho_e}{\partial \xi_{i\tau}} \rho_e^\alpha \hat{\mathbf{u}}^{\text{T}} \hat{\mathbf{L}}_e^{\text{T}} \mathbf{K}_e^0 \hat{\mathbf{L}}_e \hat{\mathbf{u}} \\ &= \sum_{e \in \mathcal{S}_\tau} \frac{\alpha}{\rho_e} \frac{\partial \rho_e}{\partial \xi_{i\tau}} \mathbf{u}_e^{\text{T}} \mathbf{f}_e = \sum_{e \in \mathcal{S}_\tau} \frac{\alpha}{\rho_e} \frac{\partial \rho_e}{\partial \xi_{i\tau}} w_e,\end{aligned}\tag{A.6}$$

where  $\mathbf{u}_e, \mathbf{f}_e \in \mathbb{R}^{N_{\text{DOF}}^e}$  are the generalised nodal displacements and forces of element  $e$ , while  $w_e$  is the work of internal forces of element  $e$  of Eq. (24).

The expressions of  $\frac{\partial \mathbf{K}}{\partial \xi_{i\tau}}$  and  $\frac{\partial \mathbf{K}_{\text{BC}}}{\partial \xi_{i\tau}}$  can be derived by applying Def. 3.1 to the derivative of Eq. (17) as follows:

$$\begin{aligned}\frac{\partial \hat{\mathbf{K}}}{\partial \xi_{i\tau}} &= \sum_{e \in \mathcal{S}_k} \frac{\alpha}{\rho_e} \frac{\partial \rho_e}{\partial \xi_{i\tau}} \hat{\mathbf{L}}_e^{\text{T}} \mathbf{K}_e \hat{\mathbf{L}}_e, \\ \frac{\partial \mathbf{K}}{\partial \xi_{i\tau}} &= \mathfrak{R} \left( \frac{\partial \hat{\mathbf{K}}}{\partial \xi_{i\tau}}, \mathcal{I}_{\text{BC}}, \mathcal{I}_{\text{BC}} \right) = \sum_{e \in \mathcal{S}_k} \frac{\alpha}{\rho_e} \frac{\partial \rho_e}{\partial \xi_{i\tau}} \mathfrak{R} \left( \hat{\mathbf{L}}_e^{\text{T}}, \mathcal{I}_{\text{BC}}, \emptyset \right) \mathbf{K}_e \mathfrak{R} \left( \hat{\mathbf{L}}_e, \emptyset, \mathcal{I}_{\text{BC}} \right), \\ \frac{\partial \mathbf{K}_{\text{BC}}}{\partial \xi_{i\tau}} &= \mathfrak{R} \left( \frac{\partial \hat{\mathbf{K}}}{\partial \xi_{i\tau}}, \mathcal{I}_{\text{BC}}, \mathcal{I}_{\text{U}} \right) = \sum_{e \in \mathcal{S}_k} \frac{\alpha}{\rho_e} \frac{\partial \rho_e}{\partial \xi_{i\tau}} \mathfrak{R} \left( \hat{\mathbf{L}}_e^{\text{T}}, \mathcal{I}_{\text{BC}}, \emptyset \right) \mathbf{K}_e \mathfrak{R} \left( \hat{\mathbf{L}}_e, \emptyset, \mathcal{I}_{\text{U}} \right).\end{aligned}\tag{A.7}$$

By taking into account for Eqs. (A.7) and (25), it is easy to check that the following equality holds:

$$\begin{aligned}\mathbf{u}_0^{\text{T}} \left( \frac{\partial \mathbf{K}}{\partial \xi_{i\tau}} \mathbf{u} + \frac{\partial \mathbf{K}_{\text{BC}}}{\partial \xi_{i\tau}} \mathbf{u}_{\text{BC}} \right) &= \\ &= \sum_{e \in \mathcal{S}_k} \frac{\alpha}{\rho_e} \frac{\partial \rho_e}{\partial \xi_{i\tau}} \mathbf{u}_0^{\text{T}} \mathfrak{R} \left( \hat{\mathbf{L}}_e^{\text{T}}, \mathcal{I}_{\text{BC}}, \emptyset \right) \mathbf{K}_e \left[ \mathfrak{R} \left( \hat{\mathbf{L}}_e, \emptyset, \mathcal{I}_{\text{BC}} \right) \mathbf{u} + \mathfrak{R} \left( \hat{\mathbf{L}}_e, \emptyset, \mathcal{I}_{\text{U}} \right) \mathbf{u}_{\text{BC}} \right] \\ &= \sum_{e \in \mathcal{S}_k} \frac{\alpha}{\rho_e} \frac{\partial \rho_e}{\partial \xi_{i\tau}} \mathbf{u}_0^{\text{T}} \hat{\mathbf{L}}_e^{\text{T}} \mathbf{K}_e \hat{\mathbf{L}}_e \hat{\mathbf{u}} = \sum_{e \in \mathcal{S}_k} \frac{\alpha}{\rho_e} \frac{\partial \rho_e}{\partial \xi_{i\tau}} \mathbf{u}_{e0}^{\text{T}} \mathbf{f}_e.\end{aligned}\tag{A.8}$$

Finally, by injecting Eqs. (A.6) and (A.8) into Eq. (A.5), one can easily retrieve Eq. (23)

and this last passage concludes the proof. ■

## B. Gradient of the generalised compliance under mixed boundary conditions

The proof of Prop. 3.2 is provided here below. Conceptually, it follows the same rationale used for the proof of Prop. 3.1.

*Proof.* Considering Eq. (15), the generalised compliance of Eq. (22) can be written as follows:

$$\mathcal{C} = \mathbf{f}^T \mathbf{u} - \mathbf{u}_{\text{BC}}^T \mathbf{r} + \boldsymbol{\eta}^T (\mathbf{K} \mathbf{u} + \mathbf{K}_{\text{BC}} \mathbf{u}_{\text{BC}} - \mathbf{f}) + \boldsymbol{\lambda}^T (\mathbf{K}_{\text{BC}}^T \mathbf{u} + \tilde{\mathbf{K}} \mathbf{u}_{\text{BC}} - \mathbf{r}), \quad (\text{B.9})$$

where  $\boldsymbol{\eta} \in \mathbb{R}^{N_{\text{DOF}}}$  and  $\boldsymbol{\lambda} \in \mathbb{R}^{N_{\text{BC}}}$  are two arbitrary vectors. Under the hypothesis that vectors  $\mathbf{f}$  and  $\mathbf{u}_{\text{BC}}$  do not depend on the TV, the derivative of Eq. (B.9) reads:

$$\begin{aligned} \frac{\partial \mathcal{C}}{\partial \xi_{i\tau}} = & \mathbf{f}^T \frac{\partial \mathbf{u}}{\partial \xi_{i\tau}} - \mathbf{u}_{\text{BC}}^T \frac{\partial \mathbf{r}}{\partial \xi_{i\tau}} + \\ & + \boldsymbol{\eta}^T \left( \frac{\partial \mathbf{K}}{\partial \xi_{i\tau}} \mathbf{u} + \mathbf{K} \frac{\partial \mathbf{u}}{\partial \xi_{i\tau}} + \frac{\partial \mathbf{K}_{\text{BC}}}{\partial \xi_{i\tau}} \mathbf{u}_{\text{BC}} \right) + \\ & + \boldsymbol{\lambda}^T \left( \frac{\partial \mathbf{K}_{\text{BC}}^T}{\partial \xi_{i\tau}} \mathbf{u} + \mathbf{K}_{\text{BC}}^T \frac{\partial \mathbf{u}}{\partial \xi_{i\tau}} + \frac{\partial \tilde{\mathbf{K}}}{\partial \xi_{i\tau}} \mathbf{u}_{\text{BC}} - \frac{\partial \mathbf{r}}{\partial \xi_{i\tau}} \right). \end{aligned} \quad (\text{B.10})$$

In Eq. (B.10), vectors  $\boldsymbol{\eta}$  and  $\boldsymbol{\lambda}$  can be chosen such that the terms multiplying  $\frac{\partial \mathbf{u}}{\partial \xi_{i\tau}}$  and  $\frac{\partial \mathbf{r}}{\partial \xi_{i\tau}}$  vanish, i.e.

$$\begin{aligned} \boldsymbol{\lambda} &= -\mathbf{u}_{\text{BC}}, \\ \mathbf{K} \boldsymbol{\eta} &= -\mathbf{f} - \mathbf{K}_{\text{BC}} \boldsymbol{\lambda} = -\mathbf{f} + \mathbf{K}_{\text{BC}} \mathbf{u}_{\text{BC}} = -\mathbf{K} \mathbf{u}, \Rightarrow \boldsymbol{\eta} = -\mathbf{u}. \end{aligned} \quad (\text{B.11})$$

By injecting Eq. (B.11) in Eq. (B.10) and by considering Eq. (A.6) one obtains:

$$\begin{aligned} \frac{\partial \mathcal{C}}{\partial \xi_{i\tau}} &= -\mathbf{u}^T \frac{\partial \mathbf{K}}{\partial \xi_{i\tau}} \mathbf{u} - 2\mathbf{u}^T \frac{\partial \mathbf{K}_{\text{BC}}}{\partial \xi_{i\tau}} \mathbf{u}_{\text{BC}} - \mathbf{u}_{\text{BC}}^T \frac{\partial \tilde{\mathbf{K}}}{\partial \xi_{i\tau}} \mathbf{u}_{\text{BC}} \\ &= -\hat{\mathbf{u}}^T \frac{\partial \hat{\mathbf{K}}}{\partial \xi_{i\tau}} \hat{\mathbf{u}} = - \sum_{e \in \mathcal{S}_\tau} \frac{\alpha}{\rho_e} \frac{\partial \rho_e}{\partial \xi_{i\tau}} w_e, \end{aligned} \quad (\text{B.12})$$

which ends the proof. ■

## References

- [1] M. Bendsøe, N. Kikuchi, Generating optimal topologies in structural design using a homogenization method, *Computer Methods in Applied Mechanics and Engineering* 71 (1988) 197–224.
- [2] M. Bendsøe, O. Sigmund, *Topology Optimization - Theory, Methods and Applications*, Springer-Verlag Berlin Heidelberg, 2004.

- [3] J. A. Sethian, *Level Set Methods and Fast Marching Methods - Evolving interfaces in computational geometry, fluid mechanics, computer vision, and materials science*, Cambridge University Press, 1999.
- [4] G. Allaire, F. Jouve, A.-M. Toader, Structural optimization using sensitivity analysis and a level-set method, *Journal of Computational Physics* 194 (1) (2004) 363 – 393.
- [5] M. Y. Wang, X. Wang, D. Guo, A level set method for structural topology optimization, *Computer Methods in Applied Mechanics and Engineering* 192 (1) (2003) 227 – 246.
- [6] M. de Ruiter, F. van Keulen, Topology optimization using a topology description function, *Structural and Multidisciplinary Optimization* 26 (6) (2004) 406–416.
- [7] Y. Xie, G. Steven, A simple evolutionary procedure for structural optimization, *Computers & Structures* 49 (5) (1993) 885 – 896.
- [8] X. Yang, Y. Xie, G. Steven, O. Querin, Bidirectional evolutionary method for stiffness optimization, *AIAA Journal* 37 (1999) 1483–1488.
- [9] Y. M. Huang, X. and Xie, Evolutionary topology optimization of continuum structures with an additional displacement constraint, *Structural and Multidisciplinary Optimization* 40 (2009) 409.
- [10] X. Huang, M. Xie, *Evolutionary Topology Optimization of Continuum Structures: Methods and Applications*, John Wiley & Sons, 2010.
- [11] X. Guo, W. Zhang, W. Zhong, Doing Topology Optimization Explicitly and Geometrically—A New Moving Morphable Components Based Framework, *Journal of Applied Mechanics* 81 (8) (2014).
- [12] W. Zhang, J. Chen, X. Zhu, J. Zhou, D. Xue, X. Lei, X. Guo, Explicit three dimensional topology optimization via moving morphable void (mmv) approach, *Computer Methods in Applied Mechanics and Engineering* 322 (2017) 590–614.
- [13] G. Costa, M. Montemurro, J. Pailhès, A 2D topology optimisation algorithm in NURBS framework with geometric constraints, *International Journal of Mechanics and Materials in Design* 14 (4) (2018) 669–696.
- [14] G. Costa, M. Montemurro, J. Pailhès, NURBS Hypersurfaces for 3D Topology Optimisation Problems, *Mechanics of Advanced Materials and Structures* 28 (7) (2021) 665–684.
- [15] T. Rodriguez, M. Montemurro, P. Le Texier, J. Pailhès, Structural Displacement Requirement in a Topology Optimization Algorithm Based on Isogeometric Entities, *Journal of Optimization Theory and Applications* 184 (2020) 250–276.
- [16] G. Costa, M. Montemurro, J. Pailhès, Minimum Length Scale Control in a NURBS-based SIMP Method, *Computer Methods in Applied Mechanics and Engineering* 354 (2019) 63–989.
- [17] G. Costa, M. Montemurro, J. Pailhès, N. Perry, Maximum length scale requirement in a topology optimisation method based on NURBS hyper-surfaces, *CIRP Annals* 68 (1) (2019) 153–156.

- [18] G. Costa, M. Montemurro, Eigen-frequencies and harmonic responses in topology optimisation : a CAD-compatible algorithm, *Engineering Structures* 214 (2020) 110602.
- [19] M. Montemurro, K. Refai, A topology optimization method based on non-uniform rational basis spline hyper-surfaces for heat conduction problems, *Symmetry* 13 (5) (2021) 888.
- [20] M. Montemurro, G. Bertolino, T. Roiné, A general multi-scale topology optimisation method for lightweight lattice structures obtained through additive manufacturing technology, *Composite Structures* 258 (2021) 113360.
- [21] T. Roiné, M. Montemurro, J. Pailhès, Stress-based topology optimization through non-uniform rational basis spline hyper-surfaces, *Mechanics of Advanced Materials and Structures* (2021). doi:10.1080/15376494.2021.1896822.
- [22] G. Costa, M. Montemurro, J. Pailhès, A general hybrid optimization strategy for curve fitting in the non-uniform rational basis spline framework, *Journal of Optimization Theory and Applications* 176 (1) (2017) 225–251.
- [23] G. Bertolino, M. Montemurro, N. Perry, F. Pourroy, [An Efficient Hybrid Optimisation Strategy for Surface Reconstruction](#), *Computer Graphics Forum*, (2021). URL <https://doi.org/10.1111/cgf.14269>
- [24] P. Pedersen, N. L. Pedersen, Design objectives with non-zero prescribed support displacements, *Structural and Multidisciplinary Optimization* 43 (2011) 205–214.
- [25] F. Niu, S. Xu, G. Cheng, A general formulation of structural topology optimization for maximizing structural stiffness, *Structural and Multidisciplinary Optimization* 43 (2011) 561–572.
- [26] A. Klarbring, N. Strömberg, A note on the min-max formulation of stiffness optimization including non-zero prescribed displacements, *Structural and Multidisciplinary Optimization* 45 (2012) 147–149.
- [27] C. Barbarosie, S. Lopes, A generalized notion of compliance, *Compte Rendus Mécanique* 339 (2011) 641–648.
- [28] L. Piegl, W. Tiller, *The NURBS book*, Springer-Verlag, Berlin, Heidelberg, New York, 1997.
- [29] K. Svanberg, A class of globally convergent optimization methods based on conservative convex separable approximations, *SIAM Journal of Optimization* 12 (2002) 555–573.
- [30] R. M. Jones, *Mechanics of composite materials*, McGraw-Hill, 1975.
- [31] R. M. Errico, What is an adjoint model?, *Bulletin of the American Meteorological Society* 78 (11) (1997) 2577–2592.